AALBORG UNIVERSITET

9th and 10th semester Drug & Tissue Technology
Department of Health Science and Technology
Fredrik Bajers Vej 7D2
Phone 99 40 99 40
Fax 98 15 40 08
http://www.hst.aau.dk

Title:
Use of Nano- and Microtopographies for Controlled Cellular Responses

Project period:
P9, The Fall Semester 2008
P10, The Spring Semester 2009

Project group:
1088d

Author:
Steffan Foldberg Nielsen

Supervisor:
Vladimir Zachar

Secondary Supervisor:
Peter Fojan[a]

Numbers printed: 4

Number of pages: 83

Number of appendices: 3

Finished: 4th of June 2009

Synopsis:

Cells in their natural environment are surrounded by extracellular nano- and microstructures. These are, together with biochemical cues, essential for directing and maintaining cellular functions and fates, such as migration, survival, proliferation, protein activity, differentiation and death. In this study, the effect of an altered extracellular topography on stem cells in culture is examined. Three sets of surfaces were produced, characterized and tested in accordance to some predefined biological parameters. These were oxygen plasma etched polystyrene surfaces, honeycomb patterned PLA surfaces and pectin scaffolds. The biological parameters included cell morphology during spreading, cell proliferation/viability and expression of some lineage, adhesion and signaling related genes. Furthermore, the surfaces were tested for their cellophilicity by evaluating their protein adsorption properties. The results showed that these three surfaces had significant impact on the cellular behavior. Specifically the plasma surfaces seemed to influence the gene expression of the cultured cells as well as the morphology. The honeycomb surfaces influenced the spreading morphology of the cells without any changes in the probed gene expression. Lastly, the pectin scaffolds had to go through several fabrication enhancements before they were stable during cell culture conditions.

[a] *Associate professor at the Department of Physics and Nanotechnology*

Preface

This master project was conducted with the main purpose of investigating how extracellular topographies could influence the cellular behavior of stem cells in culture. This was done by evaluating biological parameters such as spreading, proliferation and gene expression. In addition, protein adsorption properties of the different surfaces were investigated in order to see if an altered substrate topography could be translated into alterations at protein level.

Three different sets of surfaces have been produced, characterized and tested in relation to the aforementioned biological parameters. These were oxygen plasma etched surfaces, polylactic acid honeycomb surfaces and pectin based scaffolds. Regarding the honeycomb and pectin surfaces, effort was also put into culture system design.

The report can roughly be divided into 4 essential chapters, namely introduction, materials and methods, results and discussion. The introduction can further be divided into a background section, that contains some general introduction to the topic, and a literature review section, which contains the more specific project related background information as well as the key studies for each field.

The report was conducted by Steffan Foldberg Nielsen during the 9th and 10th semester specialization 2008/2009 in Drug & Tissue Technology at the Institute for Health Science and Technology, Aalborg University. During the project, several people have given essential feedback and assistance. Therefore I would like to thank Julia Wilke for assistance in testing proliferation, spreading and ELISA on the plasma etched surfaces. Leonid Gurevich for assistance with SEM and AFM. Jens Rafaelsen for help with SEM and EDS analysis. Helle Møller and Trine Fink for introduction to and assistance with real-time qPCR and Merete Fredsgaard, Mayuri Prasad, Linda Pilgaard and Pia Lund for providing positive control RNA for lineage-specific genes for real-time qPCR. Morten Petersen for general discussions regarding the project.

Throughout this project several abbreviations have been used for appendix (App.), equation (Eq.), figure (Fig.), section (Sec.) and table (Tab.). References are shown in the text as numbers enclosed in square brackets, and the bibliography can be found at the end of this report. Furthermore, a digital copy of the report as well as the references can be found on the enclosed CD.

Steffan Foldberg Nielsen

Abbreviations

AFM	-	Atomic Force Microscopy
App.	-	Appendix
ASCPx	-	Adipose tissue derieved Stem Cell, Passage no. x
ASK	-	Apoptosis Signal-regulating Kinase
bmMSC	-	Bone Marrow derived Mesenchymal Stem Cell
BSA	-	Bovine Serum Albumin
CAM	-	Cell Adhesion Molecule
ECM	-	ExtraCellular Matrix
EDC/NHS	-	Ethyl(dimethylaminopropyl) carbodiimide/N-Hydroxysuccinimide
EDS	-	Electron-Dispersive x-ray Spectroscopy
ELISA	-	Enzyme-Linked ImmunoSorbent Assay
Eq.	-	Equation
ERK	-	Extracellular signal-Regulated Kinase
FA	-	Focal Adhesion
FAK	-	Focal Adhesion Kinase
Fig.	-	Figure
GAG	-	Glycosaminoglycans
hESC	-	Human Embryonic Stem Cell
ILK	-	Integrin-Linked Kinase
IRAK	-	Interleukin-1 Receptor-Associated Kinase
JNK	-	c-Jun NH2 terminal Kinase
MAPK	-	Mitogen Activated Protein Kinase
MEK	-	MAPK Kinase
PAK	-	p21-Activated Kinase
PCM	-	Phase Contrast Microscopy
qPCR	-	Quantitative Polymerase Chain Reaction
PePSx	-	Plasma etched PolyStyrene, x minutes
PI3K	-	Phosphoinositide 3 Kinase
PKB	-	Protein Kinase B
PLA	-	PolyLactic Acid
PS	-	Polystyrene
Rho	-	Subfamily of the RAS superfamily
ROCK	-	Rho Kinase
RT	-	Room Temperature
SC	-	Stem Cell
Sec.	-	Section
SEM(1)	-	Scanning Electron Microscopy
SEM(2)	-	Standard Error of Mean
PBS	-	Phosphate Buffered Saline
Tab.	-	Table

Contents

1

Introduction

The use of stem cells (SCs) in medical treatments may benefit millions of people worldwide. Today many diseases can be treated or held at a stage where a patient can live an almost normal life with the same wellbeing as his fellow human beings. However, some diseases are so debilitating that current treatments only slow down the inevitable signs and symptoms, and often with the possibility of suffering from severe treatment-related side-effects. These debilitating diseases, such as Alzheimer, Parkinson, diabetes, cancer and myocardial infarction are all characterized by relatively deficient treatments in terms of curing the patient. So where these treatments often focus on treating the symptoms of a patient, rather than the actual disease, SC treatments elicit extraordinary regenerative potential of the human body. However, before SCs can be applied in the clinic, the cellular mechanism has to be harnessed and tailored to the specific treatment.

Cells in their natural environment are surrounded by many geometrically different micro- as well as nanostructures, e.g. fibers, pores, crystals etc. It is known today that these extracellular topographical cues have an important impact on cellular function. Because of the complexity of these cells, researchers try to learn from cells in their natural environment and apply this to control the fate of the cells. This could be in terms of maintaining the stemness, or by differentiating the cells along a specific lineage. The understanding of how cells interact with these topographies could help the engineers to design and improve already existing implants with physicochemical and biological properties that resemble those of native tissue.

To begin with, focus for this research field was on microscale topographies, which were produced with techniques that came with the advent of the silicon microelectronics industry. However, when moving into the nano domain, small modifications in topography appear to have tremendous impact on the cellular responses.

This leads to the initiating problem for this study, namely:

> How can the cellular machinery be harnessed through the use of substratum micro- or nanotopographies?

1.1 Stem Cells

The term 'stem cell' has existed for more than one hundred years and was first used in relation to blood cells, as the Russian histologist Alexander Maximov proposed that the various types of specialized blood cells all derived from the same master cell - the haematopoietic stem cell [1]. This important discovery lead to the use of bone marrow transplantations, which still is used today in treatments for various diseases, e.g. cancer. The official definition of a SC is according to the National Institutes of Health (NIH)[2]:

> A stem cell is a cell from the embryo, fetus, or adult that has, under certain conditions, the ability to reproduce itself for long periods or, in the case of adult stem cells, throughout the life of the organism. It also can give rise to specialized cells that make up the tissues and organs of the body.

This quote summarizes the two most important characteristics of a SC, namely its ability to reproduce itself indefinitely, or at least for a long period of time, and its potential to differentiate into more specialized cells of the organism. There are different types of SCs, which can be classified by their potential to differentiate into various tissues. In this regard, cells can be classified by being either totipotent (able to give rise to all embryonic and extra-embryonic cell types), pluripotent (able to give rise to all cells of all three germ layers), multipotent (able to differentiate into a number of cell lineages within one germ layer) or unipotent (committed to one lineage) [2–4]. The physiological totipotent SC is the fertilized egg (zygote) or the first blastomers during embryonic development, whereas pluripotent embryonic SCs are derived from the inner cell mass of the blastocyst. As these cells loose their toti- and pluripotency and become more committed during embryo development, they are not available for autologous transplantations in adults, and the use of these cells from embryos is furthermore intertwined with a substantial ethical debate.

On the contrary, adult SCs constitute a group of cells, which is set aside during early development, and thus can be found in any adult person, which allows for cell-based therapies using autologous transplantations. Adult SCs are multi- or unipotent and have so far been isolated from a variety of tissues. Bone marrow and brain derived SCs are the most studied, however the list of SC niches increases continuously [2, 5].

The most abundant and easiest accessible source of adult SCs is adipose tissue derived SCs (ASCs), which are characterized by an immunophenotype resembling that of bone marrow derived SCs (bmMSCs), see Tab.(1.1). ASCs have furthermore shown multilineage differentiation potential, including the chondrogenic, myogenic, osteogenic and adipogenic lineages. In addition, ASCs have shown capabilities to transdifferentiate into the neuronal and epithelial cell lineages [6, 7].

Table 1.1: The phenotypic profiles of human bone marrow derived SCs and adipose tissue derived SCs. Compiled from [5–10].

Antigen	bmMSCs	ASCs
CD10 (Neprilysin)	+/-	+
CD11b (Integrin alpha M)	-	-
CD13 (Alanine aminopeptidase)	+	+

CD29 (Integrin, beta 1)	+	+
CD34	-	-
CD44 (Hyaluronate receptor)	+	+
CD45 (Protein tyrosine phosphatase, receptor type, C)	-	-
CD49d (Integrin, alpha 4)	-	+
CD49e (Integrin, alpha 5)	+	+
CD59 (Protectin)	?	+
CD90 (Thy-1)	+	+
CD106 (Vascular cell adhesion molecule 1)	+	-
CD166 (Activated leukocyte cell adhesion molecule)	+	+
HLA-ABC (Human leukocyte antigens A,B,C)	+	+

1.2 Tissue Engineering & Regenerative Medicine

Tissue and organ replacement surgeries, without the use of immunosuppressive drugs, often lead to complications because the human immune system rejects the foreign transplant. In order to circumvent an immunogenic response towards the transplant, immunosuppressive drugs are often used. However, the use of these drugs is often related with many severe side effects. For this reason, tissue engineering aims at using autologous cells in combination with suitable scaffolds, that can support the proliferating, migrating and differentiating cells. Other approaches use a biomaterial without cells, which calls for cells to migrate into the scaffold [11].

The scaffold must be designed to replicate the biological and mechanical functions of the native extracellular matrix (ECM) found in the tissue of interest. Micro- and nanoscale features are present around cells in their in vivo environment, and contribute significantly to the overall function and structure of the specific tissue [12]. An example is the basement membrane of corneal epithelium, which has a complex composition of 77 ± 44 nm wide fibers intermingled with 72 ± 40 nm wide pores that cover around 15% of the total surface area [13].

Scaffolds can either be designed for cellular or acellular treatments, and thus the interaction between cells and scaffolds, the adhesion of cells to the scaffold, cell maturation, proliferation, migration, ECM production and differentiation are all important biological parameters to consider when designing the supportive scaffold [14, 15].

1.3 Biomaterial Scaffolds

In addition to aiding mechanical support for transplanted cells, scaffolds can also be designed with more intelligent properties such as chemical and topographical cues that can be used to direct and control the cellular response. The mechanical properties are very important when fabricating a scaffold for implantation, as studies show that the biocompatibility is improved significantly when material properties approximate that of the local tissue [16].

Scaffolds designed for in vivo use are the ultimate goal of the tissue engineering process, however as many studies imply, cells can be controlled during in vitro expansion as well - either through the use of soluble factors or by the use of defined micro- or nanotopographies [17].

The interdisciplinarity of this research field is really prominent when it comes to scaffold design and characterization. This is due to the key concepts that are

related to material engineering, developmental biology, biochemistry and clinical implementation. These concepts include biocompatibility and biodegradability of the scaffold, parameters that are very material dependent. Furthermore, physicochemical parameters such as pH, oxygen tension and temperature can vary greatly in the body and in addition the body has many cyclic stresses such as heart muscle contraction and peristaltic motion of the gut. For this reason, the biomaterial must be designed with care for optimal biological properties [16].

Another significant factor to consider is cell-polymer interactions, which should be harnessed for controlling the cellular cues of the scaffold - whether it is for a acellular or cellular treatment. The cell fate and function are typically influenced by three types of interactions, the ones with soluble factors (growth factors and cytokines), the interactions with the ECM and the interactions with other cells [16].

1.3.1   Cell-polymer Interactions

In order to understand the interactions facilitating adhesion of cells to polymer materials, it is obvious to look at the mechanisms involved in cell-cell and cell-ECM interactions of the native tissue. The first thing to realize is that the cell-ECM interactions are not static, rather they are involved in a dynamic process influencing cell signaling, which again affects the ECM in multiple ways. Although cell-cell interactions are less dynamic than the cell-ECM ones, they contribute equally in cell signaling events. [17, 18]

Cell-cell interactions   are facilitated through specialized integral membrane proteins called cell-adhesion molecules (CAMs), which consists of four major families: Cadherins, immunoglobulins, integrins and selctins. These CAMs mediate the intercellular adhesions through extracellular domains, which either can be homophilic or heterophilic, meaning that the cells interact through the same kind of CAM or through different CAMs, respectively, see Fig.(1.1). Furthermore, cell-cell interactions can be direct or indirect, meaning that cells can be connected directly to each other or through interactions with the ECM. The intracellular parts of the CAMs are often connected to elements of the cytoskeleton and thus involved in activation of certain signaling pathways influencing protein activity and gene expression [18].

Cell-ECM interactions   are often described by a dynamic reciprocity, meaning that ECM molecules stimulate a response in the cell, which leads to expression of genes, whose products in turn affects the ECM back. Some cell-surface receptors can bind components of the ECM, thereby indirectly linking cells to each other or directly to the ECM. The exact composition of ECM varies greatly from tissue to tissue, however there are some universal ECM components that are involved in ECM-cell signaling. The three major classes of ECM components are proteoglycans, collagens and multiadhesive matrix proteins. Together these form a mesh of interlocking proteins, which constantly is remolded by resident cells [17, 18].

Collagens are the most abundant proteins by weight in the human body. There are 29 types described in the literature, however more than 90% of the
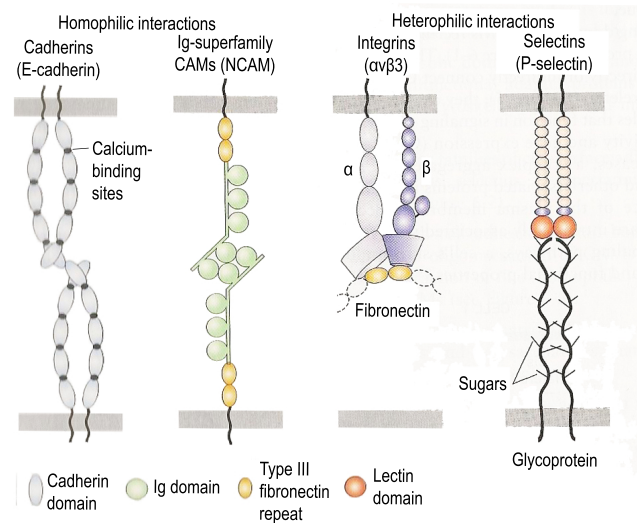
Figure 1.1: **Cell adhesion molecules (CAMs)** are cell-surface molecules that are involved in interconnection of cells, which either occurs directly or through the ECM. These CAMs are often connected to the cytoskeleton of the cell, thus directly influencing intracellular protein activity and gene expression. Modified from [18].

collagen in the human body is of type I, II, III or IV. The many types of collagen each have distinguishable characteistics, such as molecular compositions, morphological appearance and functions. Another fibrous molecule of the ECM is elastin. However, in contrast to collagen, elastin adds elasticity to tissues, allowing them to stretch when needed and return to their original shape afterwards.

Glycosaminoglycans (GAGs) are long unbranched polysaccharides composed of repeating disaccharide units. Together with a protein core, GAGs constitute proteoglycans, whose morphological appearance are rod-like with many branching GAGs, but not necessarily the same type. Proteoglycans have a net negative charge that attracts water molecules and thus keeps the ECM and cells hydrated. In native ECM, the only GAG existing without a protein core is hyaluronic acid, which is a polysaccharide composed of repeating disaccharide units of glucoronic acid and N-acetyl glucosamine.

Fibronectin, a 440 kDa disulphide-bonded dimer glycoprotein, facilitates the adhesion of cells to both other cells as well as the surrounding ECM through binding sites for collagen, integrins and heparan sulphate proteoglycans. One specific repeat in the fibronectin polypeptide is the Arg-Gly-Asp (RGD) sequence, which is recognized by certain integrins responsible for adhesion of cells.

Finally, laminin, a 820 kDa multiadhesive glycoprotein, that together with type IV collagen, entactin and perlecan constitutes the basal lamina, has domains for binding various types of collagen, polysaccharides, integrins and extracellular signaling molecules, e.g. growth factors and hormones [17–19].

11

Receptors for ECM molecules include the integrin superfamily, several transmembrane proteoglycans as well as other non-integrin receptors.

Integrins are heterodimeric transmembrane proteins composed an α and a β subunit. With 19 α and 8 β units, these can be paired in a variety of combinations, thus resulting in a large family of proteins that recognizes different parts of the ECM. Some integrin receptors are very specific, whereas others bind to several epitopes of the same ECM molecule or of different molecules. The β_2 subunit is mostly involved in cell-cell adhesions, whereas β_1 and β_3 subunits mediate cell-ECM interactions. In general, the β_1 integrins interact with ligands found in connective tissue, including fibronectin, laminin and collagen. The β_3 integrins are mostly involved in interactions with vascular ligands, including von Willebrand factor, thrombospondin, vitronectin and fibrinogen [17]. Integrin receptors can exist in a low-affinity conformation (knees bent) as well as in a high-affinity conformation (straight), which provide an explanation for how integrins can transduce both outside-in and inside-out signaling [18].

Clustering of fibronectin and vitronectin integrin receptors $\alpha_5\beta_1$ and $\alpha_V\beta_3$ leads to the formation of focal adhesions (FAs), which are specialized subcellular protein clusters that mediate ECM-cell interactions [20, 21]. FAs will be described further in the next section.

Transmembrane proteoglycans are another group of proteins that facilitate binding of cells to the ECM. One example is the syndecan family, which binds to collagens and fibronectin. In addition, the extracellular part of these proteoglycans have been shown to bind growth factors and other external signaling molecules that can modulate the cellular metabolism and function. The cytosolic part of the molecules often interacts with the actin cytoskeleton or other intracellular regulatory proteins, and thereby directly influencing cell signaling [18, 19].

Focal Adhesions and Stress Fibers

As described in the previous section, many types of cell-ECM adhesions exist, however none are as thoroughly studied as the ones involving FAs. FAs are at this point known to exist in four different subtypes, namely focal complexes, focal adhesions, fibrillar adhesions, and 3D matrix adhesions [20]. The structural organization of FAs is characterized by three major domains: Transmembrane receptors, the attached cytoskeleton and interconnecting plaque molecules as illustrated in Fig.(1.3). The transmembrane receptor domain consists mainly of members of the integrin superfamily, which has been described previously. The cytoskeletal domain consists primarily of actin filaments and a few other proteins such as α-actinin and filamin. However, the simplicity ends when it comes to the intracellular plaque molecules, which at this point are known to have more than 50 constituents [22]. Some of these plaque proteins are believed to be involved only in stabilization (vinculin, α-actinin and talin), whereas others also are involved in signaling (FAK and mitogen-activated protein kinase (MAPK), paxilin and tensin) [21, 23]. Since the specific signaling pathways are very complex and still unsolved for some molecules, it is hard to deduce the exact functions of the various components of the FA [17, 22, 24].

Formation of FAs in spreading cells is initiated by clustering of integrins combined with binding to extracellular ligands at the periphery of the spreading cell. At first, these are immature focal complexes, but as the attachment to the
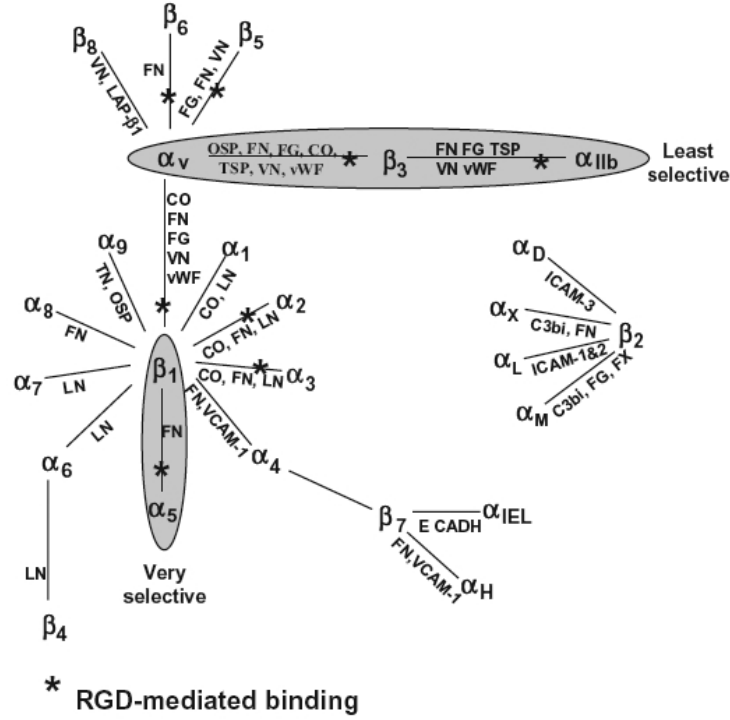
Figure 1.2: **Members of the integrin superfamily and their respective ligands.** Cell-cell interactions are mostly mediated through the β_2 subunit, while cell-ECM interactions mostly are mediated through β_1 and β_3 subunits. *Abbreviations:* Collagens (CO), Complement component (C3bi), fibrinogen (FG), fibronectin (FN), Factor X (FX), intercellular adhesion molecule x (ICAMx), laminin (LN), osteopontin (OSP), tenascin (TN), thrombospondin (TSP), vascular cell adhesion molecule-1 (VCAM-1), vitronectin (VN), von Willebrand factor (vWF), E-cadhedrin (ECADH), latent activating protein $\beta1$ (LAP$\beta1$). From [17].

extracellular ligands increases, the complexes develop into mature FAs [21]. The initial formation of the focal complexes and stress fibers is directed by the proteins Cdc42 and Rac, whereas Rho is responsible for the maturation of the FA complex - all these proteins belong to the GTPase superfamily [18, 20]. It is the spreading of the cells, combined with syndecan-4 interactions, that activates the Rho signaling, which in turn activates the Rho kinase (ROCK) to stimulate the formation of stress fibers and maturation of FA complexes [25]. Finally this maturation allows for further signaling cascades to be initiated as seen in Fig.(1.4), which will be described in Sec.(1.3.2).

1.3.2 Signaling Events During Cell-ECM Interactions

As discussed in the previous sections, ECM molecules are able to undergo specific and unspecific interactions with cell-surface receptors, which then in turn can trigger certain intracellular mechanisms and thus ultimately influence in-
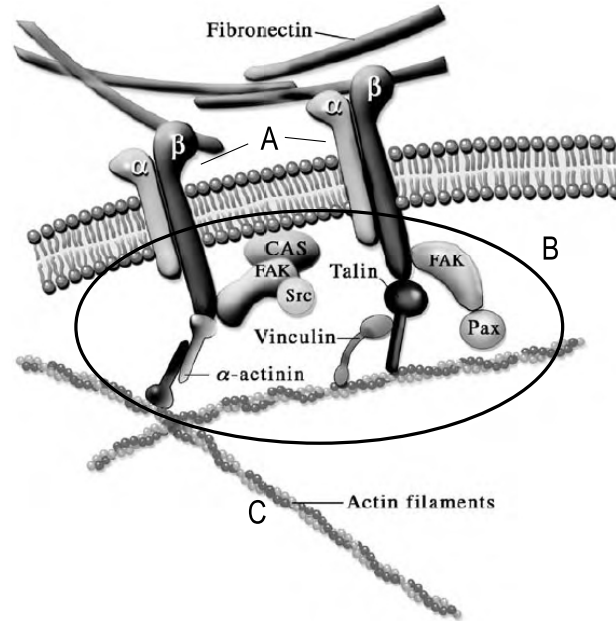
Figure 1.3: **Simplified model of a focal adhesion.** A FA can be divided into three domains: The transmembrane receptors (A), the intracellular plaque proteins (B) and the cytoskeleton (C). Modified from [24].

tracellular protein activity and gene expression. This altered expression and activity can then have impact on the functions and fate of the cell, such as migration, adhesion, cytoskeletal remodeling, proliferation, survival, cell cycle regulation or differentiation [26]. These interactions have been of interest for researchers for many years and studies on many of these interactions have been conducted. However, no interactions are described as well as those involving integrins, which is understandable, as these are the most prominent in the scope of ECM-cell signal transduction.

In general the ECM-cell interactions can occur in multiple forms, such as binding of different ECM molecules or different ECM plus growth factors etc. The versatility of these interactions makes it difficult to generalize within this topic. There are some pathways and general interactions that are known to be vital in relation to signal transduction from the ECM molecules. However, even the delimitation to individual signaling pathways quickly becomes a complex task, and therefore the presentation will be simplified substantially here.

The mitogen activated protein kinase (MAPK) pathway can be activated trough a variety of factors, such as growth factors, cell stress, ECM ligands and cytokines. The MAPKs are involved in many cellular processes from early embryonic development to cell proliferation and differentiation [27]. There are three subfamilies of the MAPK pathway, namely the extracellular signal-regulated kinase (ERK), the c-jun NH_2-terminal kinase (JNK) and the p38 enzymes [28]. The MAPK pathway can be triggered by binding of ECM molecules to integrins, which translates the signal to the focal adhesion ki-
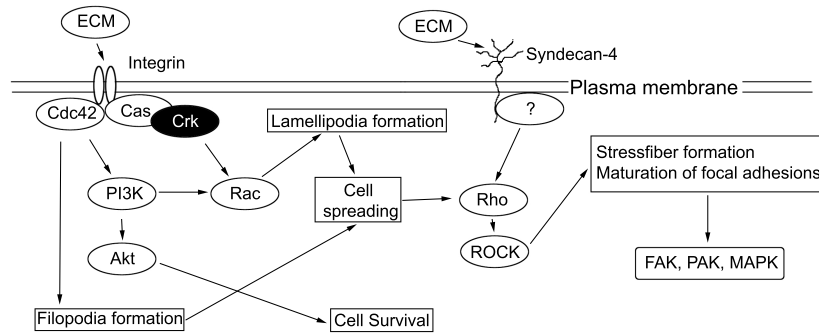
Figure 1.4: **Role of Rho in cytoskeletal formation.** The activation of small numbers of integrins initiate the Cdc42/Rac signal cascade, which leads to the formation of filopodia and lamellipodia, which together accounts for cell spreading. Spreading together with syndecan stimulation activates the Rho/ROCK signals, which eventually lead to formation of stress fibers and maturation of focal adhesions, which again act as clusters for further cell signaling.

nase (FAK) and thus initiates the MAPK/ERK pathway through the RAF or MEK1/2 molecules. However, the binding of growth factors also has the ability to initiate the MAPK/ERK by activating the Ras/Raf/MEK1/2 molecules, see Fig.(1.5). The MAPK/JNK pathway can initiated through the integrin-regulated p21-activated kinase (PAK), which can activate the ASK/MEK4/7 pathway. Lastly, the p38 subpathway is reserved for growth factor receptor initiated signaling through ASK/MEK3/6 activation. These three signaling pathways are all able to transduce an extracellular signal to the nucleus of the cell [29–31].
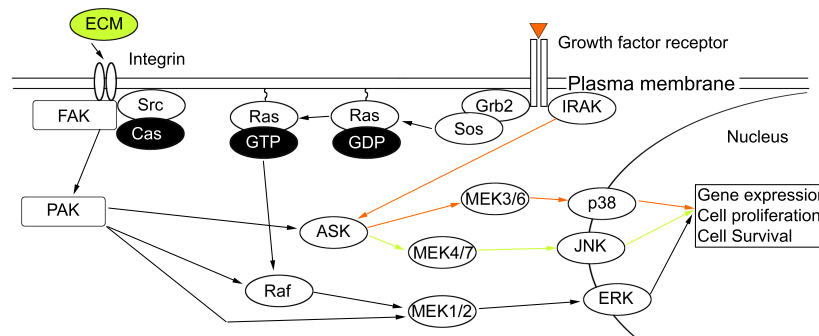
Figure 1.5: **The MAPK pathway is involved in many cellular mechanisms.** The MAPK signaling pathway can be initiated by binding of growth factors or ECM molecules, and is involved in gene expression, survival and proliferation. It is a complex pathway that can be regulated at many stages for both the growth factor and ECM induced signal.

An example of MAPK/ERK regulation is the expression of the transcription factor RUNX2, which is involved in early stages of osteogenesis. This factor is upregulated when the MAPK/ERK is initiated through the ECM interaction,

but downregulated when growth factors initiate this signal cascade [32].

The phosphoinositide-3 kinase (PI3K) pathway is a key player in relation to cell survival and proliferation. Like the MAPK pathway, it is vital for cells to avoid apoptosis and for cells to pass from the G1 to the S-phase in the cell cycle. This is illustrated in Fig.(1.6) where integrin anchorage activates the FAK, which in turn activates the integrin linked kinase (ILK). This kinase sets of the AKT/PKB signal cascade that prevents cells from undergoing apoptosis and furthermore stimulates the cell cycle progression, through inhibition of GSK3 activity. Binding of growth factors can also initiate the signal cascade through the ILK complex [33, 34].

Figure 1.6: **PI3K pathway in relation to cell survival.** Many mammalian cells are dependent on integrin-anchorage in order to survive and prolifer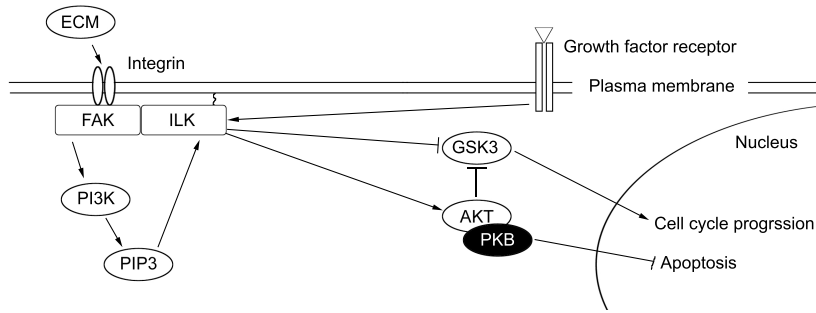ate. The PI3K pathway can transduce this extracellular binding of ECM molecules (or growth factors) to an intracellular signal that prevents cells from undergoing apoptosis and furthermore stimulate the activity of cyclins, which are necessary for cells to pass from the G1 to the S phase in the cell cycle.

1.3.3 Scales in Tissue Engineering

In order to fully understand the concept of tailoring biomaterials, it is necessary to introduce the reader to an essential scale within tissue engineering. This scale can roughly be divided into three regimes, where each regime is characterized by its unique influence on cell fate and function [35].

First we have the supracellular scale ($> 100\ \mu m$), which basically is considered inert in terms of cellular responses and typically used for arranging cells in either 2D or 3D and providing desired mechanical properties to the scaffold. This scale is very important when moving cell-based therapies into the clinic, as arrangement and organization of the cells in relation to the diseased tissue is paramount. The next regime is the cellular ($10\ \mu m$ - $100\ \mu m$), which, through chemical composition and structures, can be utilized to control the fate and function of cells. The last regime is the subcellular one ($< 10\ \mu m$), which basically targets stimulation of specific surface receptors through interaction with specific proteins. This regime is furthermore believed to have the greatest impact on biological responses. The transition from the cellular to sub-cellular scale is very diffuse and researchers still discuss the influence of micro versus nanotopographies [16, 36].

1.3.4 Fabrication of Biomaterial Scaffolds

Fabrication of biomaterial scaffolds encompass a vital component of modern tissue engineering, and many of the associated classical fabrication techniques have their origin in the silicon microelectronics industry [37, 38]. However, this is an advancing research field and many new techniques and derivatives hereof are invented regularly, which makes a complete review of this topic impossible. Therefore only a selection of technologies will be accounted for to introduce the reader to some of the vital concepts. It is important with fabrication technologies that can separate chemistry from topography in order to elucidate if cells react to chemistry or topography? However, as many processes involve other materials or elements, it is difficult to completely separate chemistry from topography.

With the aforementioned biological scales in mind, it is evident that the fabrication of a scaffold can be addressed differently, depending on the desired final properties for the particular scaffold. Other factors to consider in regard to the fabrication process, include time consumption, price, difficulty etc., which all are very important if moving into clinic. An overview of the pros and cons of the selected methods can be seen in Tab.(1.2). Classically there are two fundamental approaches in regard to nano structure fabrication, namely bottom-up and top-down. The bottom-up method utilizes physicochemical properties of materials and nature's own processes to drive the formation of self-assembling structures at the nano scale. The advantages of self-assembling systems are their resolution as well as their ease of fabrication, which is both fast, cheap and reliable. However, in order to control the process, it is necessary to engineer the materials at molecular level, which complicates this approach compared to top-down methods [39, 40].

Polymer demixing is a quick self-assembling process for creating randomly ordered nanofeatures. The process is driven by the phase separation of different polymer blends and can, to a certain extent, be controlled by varying polymer ratios and concentration. The polymer ratio influences the shape of the domains, which has been shown to form pits, islands or ribbons. Contrarily, the polymer concentration influences the size of the features [35]. This technique is hard to control in the horizontal direction, but far more reliable in the vertical direction, which has been shown to be controllable down to heights of 13 nm [41].

Phase separation involves no special equipment and easily allows for fabrication of porous and fibrous 3D structures. The process roughly consists of five steps: Polymer dissolution, phase separation and gelation, solvent extraction with water, freezing and freeze-drying. The gelation process is the critical step for controlling the pore sizes, however other parameters, such as solvent, type of polymer, polymer concentration, thermal treatment and general order of procedure can be adjusted to tailor the porosity of the scaffold [42].

The general approach in top-down methods is to start with a bulk material and then remove unwanted regions, thus ultimately ending up with the desired features. Methods in the top-down regime are typically more complete than the bottom-up ones, which mainly is due to the billion dollar investment made in the silicon semiconductor industries. The most widely used technology is, without doubt, lithography, which utilizes a prefabricated mask, a photoresist and illumination to depict a certain pattern on the desired substrate surface. Afterwards, this can be etched away (positive resist) or made etching resistant

(negative resist). However, due to the nature of light, there is an inherent lower limit for this technology, which is roughly around 1 μm [43].
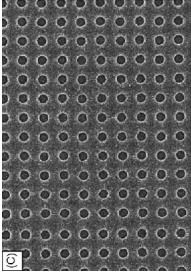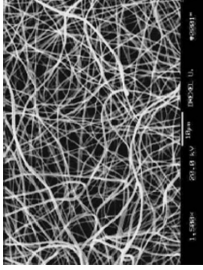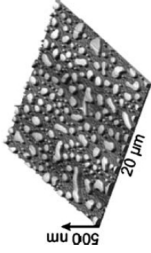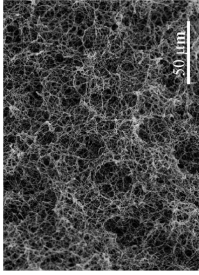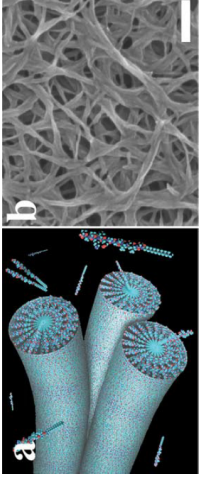
A derivative, that has taken lithography into the nanoscale domain, is electron beam lithography, which utilizes the shorter wavelength of electrons, compared to photons of the UV-VIS spectrum, to write with a much higher resolution. Furthermore, this technique does not require the use of a prefabricated mask, which allows for detailed, reproducible and easily adjustable surface patterns. However, the drawbacks of this technique are the price, time consumption and restriction to 2D [35, 44].

Electrospinning can be used to fabricate fibers ranging from a few nanometers to several hundred micrometers in diameter. The process of electrospinning involves electrical charging of the polymer solution and thus driving it through a thin capillary toward a grounded surface. The technique has been utilized with more than 50 polymer materials and can even be utilized with natural biopolymers such as collagen [45].

Etching procedures, wet and dry, are probably the most simple approach in the top-down regime and it is often used in combination with many other technologies. However, etching alone, can be used to fabricate various rough surfaces, which alone can influence the cellular behavior. An example is tissue culture polystyrene (TCPS), which differs from regular polystyrene by being etched with a highly reactive gas plasma for a short period of time [46, 47].

Table 1.2: Overview of nanoscale fabrication techniques in tissue engineering.

Technique	Features and resolution	Advantages		Disadvantages
Electron beam lithography	Single features ≥ 3-5 nm. For multiple features ≥ 30-40 nm	Precise, reproducible patterns. masks are required.	No	Time consuming, very expensive equipment is needed.
Electrospinning	Fibers. ≥ 3 nm	Easy to fabricate fibrous meshes.		Can only create fibers.
Polymer demixing	Pits, islands and ribbons. Vertical: ≥ 13 nm	Simple, fast and inexpensive.		Random organization of features.
Phase separation	Pore sizes ≥ 1 nm	Simple and reliable for producing porous matrices.		Random organization of pores.
Chemical/physical etching	Dependent on the etchant/process and time.	Simple and fast.		Specific feature geometries are not possible.
Self-assembly systems	Dependent on the system, but limit at the molecular level.	Spontaneous assembly into higher ordered structures.		Requires demanding engineering of the self-assembling molecules.

(A) E-beam lithography: 120 nm wide and 100 nm deep pits in silicon substrate. From [48].

(B) Electrospinning: PLGA nanofibrous structure composed of randomly orientated nanofibers. Scale bar 10 μm. From [49].

(C) Polymer demixing: 27 nm high islands composed of a polystyrene/poly(4-bromostyrene) blend. From [50].

(D) Phase separation: Polylactic acid microporous structure composed by phase separation of polylactic acid/Tetrahydrofuran. From [42].

(E) Self-assembly: (a) schematic representation of the assembly of individual amphiphilic peptide molecules into fibers. (b) shows the fiber assembly into a fibrous network. Scale bar 200 nm. From [51].

1.4 Literature Review

The following sections will introduce the reader to the most important publications in relation to the topic of this report, namely controlled cellular responses through the use of nano- and microscaled topographies in the extracellular environment. Furthermore, studies related to plasma etched, PLA honeycomb and pectin surfaces will be reviewed.

1.4.1 Cellular Responses to Nano- and Microtopographies

The effect of substratum topography on the cellular behavior has been a hot topic for many years now, however until recently, only one summarizing review article has been published within this field [52]. This is most likely due to the difficulty associated with the compilation of the numerous studies that have been conducted, and because both substratum material, feature type, feature size, culturing conditions, cell type and analysis methods have been varied. Martínez and co-workers [12] published a new comprehensive review in 2009, and this review summarizes the most important findings within this field. However, a review this thorough is outside the scope of this project, and thus only the most related and significant findings will be included. In general, the extracellular cues can be divided into three categories, namely chemical cues, topographical cues and those related to substrate elasticity. It is often hard to isolate one group alone, however some studies are more systematic than others, which is a key criterion for this review.

Spreading and Orientation

That cells react to microscaled grooves has been investigated in several studies [53–55], and there is a clear consensus that cells align and orientate parallel to a grooved substrate. Loesberg and coworkers [56] tested the lower limit for which human fibroblast orientated in response to a grooved substratum. They observed that for groove depths < 35 nm or widths < 100 nm no whole cell alignment occurred.

Regarding other geometries, there is less consensus between the observed responses in the various studies. Berry and co-workers [57] conducted a study to investigate the effect of microsized pits (7, 15 and 25 μm wide and 20 and 40 μm interspacing) in quarts on proliferation and spreading of cultured fibroblasts. The results clearly indicated that cells proliferated on all surfaces and even slightly faster on the surface with 7 μm wide pits. Furthermore, their results showed that cells were able to interact with the edges of the smaller pits, and when the pit diameter was increased to 25 μm, the cells were able to move into the pits. Dalby and colleagues [48] investigated the cell interactions with pits in the nanoscale and found that the filopodia of the cells interacted with pits that were 75 and 120 nm wide, but not with pits of 35 nm, thus showing a lower limit for nanotopography effects.

Choi et al 2007 [58] demonstrated the geometrical effect of silicon nano-scaled grooves and spikes. The grooves and spikes were furthermore created in various heights (from 50-600 nm), whereas the intergroove and interpit distances were constant at 230 nm. Human fibroblast cells showed significantly lower cell size and proliferation on the spiked surface, and furthermore the cells aligned parallel

on the grooved surfaces. These effects became more pronounced as the feature size increased. In addition, the cells displayed distinctive focal contact points, which on the spiked surface became more localized as spike height increased. On the grooved surface, the focal points first became elongated parallel to the grooves and secondly, as groove height increased, the whole cell became more orientated parallel to the grooves - see Fig.(1.7).
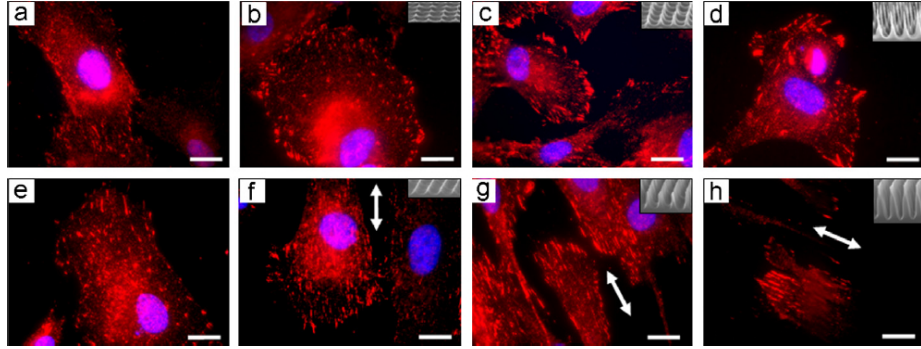
Figure 1.7: Cell adhesions and nuclei (phosphorylated focal adhesion kinase in red) of cells on the spiked surfaces (**b-d**) and grooved surfaces (**f-h**). (**a**) and (**e**) show references for spikes and grooves, respectively. The insets show the substratum topography and the arrows indicate the groove orientation of the substratum. The scale bar represents 10 μm in each image. From [58].

Proliferation

As with spreading and adhesion, proliferation is another indicator of an altered cell metabolism and thus possibly an altered cell phenotype. In the literature most studies report decreases in proliferation when cells are exposed to nanotopographies [58], however some studies show significant increases in proliferation compared to the flat reference surfaces [57, 59].

Many studies focus on the qualitative cellular responses when examining novel surface topographies and thus proliferation is not always measured. Consequently there is a lack of systematic studies investigating the effect of nanotopographies as well as the consequence of an altered cell metabolism on the further development of the cell.

One study by Kunzler et al [60] addresses cell proliferation in response to a gradient of nanoparticle density. Poly (ethylene imine)-RGD coated silicon wafers were produced with a gradient of silica nanoparticle density, ranging from 0-20% surface coverage, and with mean particle diameter of 73 nm. After 7 days of culture, the number of osteoblasts were eight times higher at positions without nanoparticles compared to positions with maximun particle surface coverage. Furthermore, the spreading and development of distinct actin networks were reduced on surfaces with maximum cell density and long filopodias were observed, indicating that cells were migrating away from the areas. The authors hypothesized that the reduced proliferation and spreading on surfaces with maximum density was a consequence of limited space for integrin bindings.
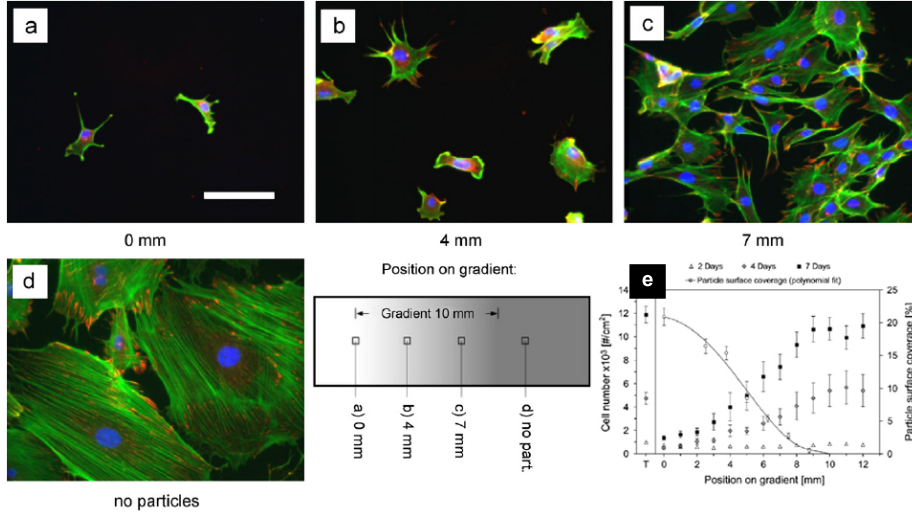
Figure 1.8: Spreading and proliferation of osteoblasts on a nanoparticle-density gradient. **(a-d)** show the spreading (actin and vinculin) of cells cultured on the gradient of nanoparticles. **(e)** shows the cell density after 2, 4 and 7 days of culture and the particle surface coverage as function of gradient position. Modified from [60].

Differentiation

There are only a few studies that demonstrate actual differentiation of SCs due to substratum topography. As with proliferation, there is a lack of systematic studies, which isolate the topography part of the culturing environment. Dalby and co-workers [61] found that bone marrow derived hMSCs not only react to the feature types of the substratum, but also sense the symmetry and disorder of the surfaces. More specifically, 120 nm wide and 100 nm deep pits were created in a PMMA substratum with varying degrees of interpit distance and positioning (symmetry/disorder). hMSCs were cultured on the various surfaces in basal medium for 21 days, after which the cells were stained for presence of calcium (alizarin red), osteopontin and osteonectin - see Fig.(1.9). The experiment showed that cells on surfaces, with a specific substrate symmetry, spontaneously differentiated into bone-like phenotypes.

Besides topography, cells are regulated through substrate elasticity, which affects cytoskeletal tension. Engler et al [62] showed that hMSCs respond to the elasticity of the substratum with extreme sensitivity. Consequently, soft matrices, resembling the elasticity of native neural tissue, were neurogenic, whereas harder matrices with elasticities similar to that of native muscle ECM were myogenic. Lastly rigid matrices, mimicking bone ECM, showed to be osteogenic. In addition, Engler et al showed that cells can be reprogrammed chemically in the initial culturing period, but after several weeks in culture, the cells commit to the lineage specified by the substratum elasticity.

McBeath et al [63] showed that lineage commitment of hMSCs was regulated by cell shape, where round cells were adipogenic and flattened cells were osteogenic. The cell shape is translated to lineage commitment through the in-
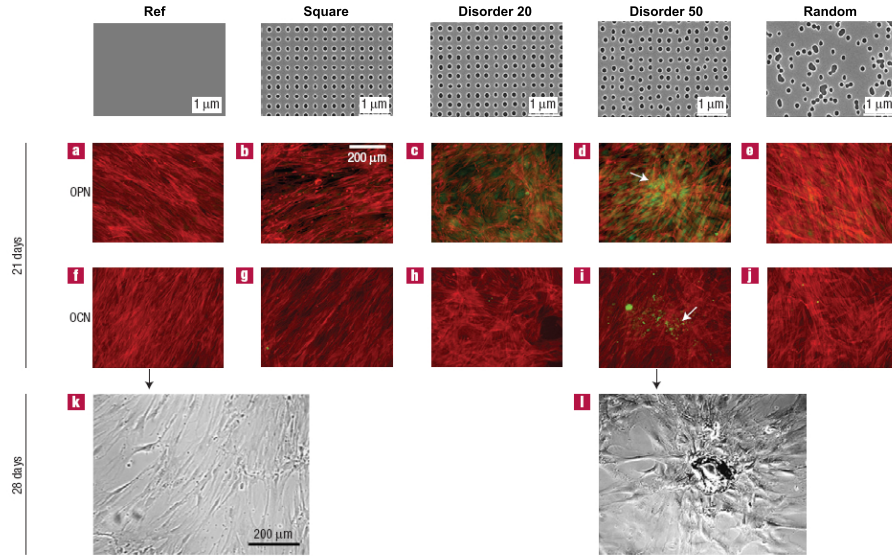
Figure 1.9: Calcium, osteopontin and osteonectin stained hMSCs after 21 days of culture. The top row shows e-beam lithography created pits in PMMA surfaces with varying degrees of symmetry/disorder. **(a-e)** show the osteopontin expression, whereas **(f-j)** show the osteonectin expression. **(k)** shows a phase contrast image of the fibroblast morphology of the reference cells after 28 days. **(l)** shows a phase contrast image of the appearance of mature bone nodules after 28 days. Modified from [61].

tracellular RhoA and ROCK signaling pathways, that for cells with osteogenic fates are upregulated. They furthermore found that the RhoA-ROCK signaling pathway is dominant over soluble induction factors, e.g. stimulation of cells to upregulate RhoA induced osteogenesis, even under adipogenic conditions.

Popat and colleagues [59] showed that differentiation of mouse MSCs into osteoblasts was increased by 50% based on matrix production when cultured on nano-porous alumina surfaces compared to culturing on flat alumina. Leong and co-workers [64] demonstrated that 3D polymer-ceramic composite scaffolds of PLGA and bioactive glass stimulate differentiation of hMSCs into osteoblast phenotypes.

1.4.2 Oxygen Plasma Etched Polystyrene

TCPS is considered the golden standard material within modern cell culturing. These surfaces have been modified to optimize the cell spreading and proliferation, however as TCPS has little resemblance to native tissues, it is questionable whether TCPS is the best suitable surface for differentiation of cells in vitro? Consequently it could be of great interest to investigate if introduction of nanoroughness to the TCPS surfaces can influence the cellular response.

Random roughness can be introduced through etching, which either can be done using a wet or dry setup. Wet refers to the use of chemicals and dry, also known as glow discharge, refers to the use of highly reactive plasma. Glow discharge is a highly controllable process, which utilizes high energy ions (plasma) to drive some reaction chemistry at the bombarded surface. Thus, in addition to random deformation of the surface due to high energy bombardments, plasma can be used to introduce molecules into the specimen, and therefore oxygen plasma eventually introduces oxygen atoms into the surface of the wafer [43].

Furthermore, the glow discharge method is applied industrially for some cell culturing products to turn otherwise unsuitable plastics into good surfaces that allow attachment and proliferation of anchorage dependent cells. Untreated polystyrene is such a material, which before glow discharge results in rounding and apoptosis of sedimented cells [47, 65]. Glow discharge can be used to increase the wettability (decrease contact angle between water droplet and surface), which greatly influences the biological properties of the surface [66]. Van Kooten et al[67] produced polystyrene surfaces with different degrees of wettability and without altering the surface roughness significantly. Their results indicated that cell proliferation increased with increasing wettability of polystyrene and furthermore, that cell proliferation was dependent on the amount of oxygen incorporated into the surfaces. Lastly they found that expression of RhoA, FAK and cadherin-5 increased for surfaces with higher wettability, which indicated that cells formed more and stronger focal adhesions as well as cell-cell interactions.

Preliminary results by our group indicated that ASCs adapted a more spindle-shaped morphology when cultured on TCPS surfaces that were etched under oxygen plasma for 5 min at a pressure of 100 $mTorr$, RF of 300 W and a oxygen flow of 40 $sccm$ [68]. This further adds to the interest for testing these surfaces.

1.4.3 Honeycomb Polylactic Acid

Polylactic acid (PLA) is a biodegradable linear polyester, which is made from organic resources, such as corn and sugar beets. Due to the chirality of PLA, it can exist in three stereoisomeric forms: L-lactide, D-lactide and meso-lactide. The mixing ratio of these influences the crystalinity, melting temperature, glass transition temperature and biodegradation of the end polymer, meaning that this versatile polymer can be engineered to large number of applications [69]. The environmental degradation of PLA occurs through hydrolysis where high molecular polyester chains are hydrolyzed into shorter chains. The shorter chains can be broken further down by microorganisms, and thus eventually the polymer will be broken down to carbon dioxide, water and humus [70].

Honeycomb patterned films have been suggested to be useful scaffolds in tissue engineering, and simple methods have been established for producing

these films [71, 72]. The formation of pores requires a surfactant that can stabilize the water droplets that constitute a scaffold for emerging pores. Initial research groups applied a synthetic amphiphilic poly acrylamide copolymer (CAP) as surfactant. However, as the metabolic pathway is not known for CAP, other groups have been searching for a natural substitute. Fukuhira and colleagues [73] tested a wide range of natural amphiphilic surfactants and found that dioleoylphosphatidylethanolamine (DOPE), a phospholipid with unsaturated fatty acid moieties, were suitable for honeycomb fabrication in PLA. They were able to produce microsized pores ranging from 4-9 μm in diameter by varying the DOPE-to-PLA ratio. Lastly they report that in general the pore sizes are influenced by temperature, humidity, gas flow rate, casting volume and casting concentration.

In another study by Fukuhira et al [74], the effect of microsized honeycomb patterned substratum on chondrocyte behavior was evaluated. The results indicated that flat PLA surfaces are better for chondrocytes in terms of proliferation, however the cells were flat and fibroblast like. Although chondrocytes proliferated slower on PLA honeycomb, they maintained a more natural rounded shape and showed a significantly higher ECM production.

In addition, other groups have established the effect of honeycomb patterned surfaces on cardiac myocytes [75], hepatocytes [76], osteoblast-like cells [77] and endothelial cells [78].

To understand the effect of honeycomb patterned substratum on cells, protein adsorption patterns have been investigated as well [78]. Sunami et al [79] found that fibronectin adhered selectively to the pores of the honeycomb film, whereas it hardly adhered to flat films. Furthermore, albumin showed non-specific adhesion to both flat as well as honeycomb films.

1.4.4 Pectin

The use of hydrogels in tissue engineering has many applications, as gels can be produced under mild conditions with physical and biological properties resembling that of native tissues. The mild conditions for the fabrication process allows for encapsulation of cells during the process, which could open for new treatments. Furthermore, the gelling mechanism can be precisely controlled for many polymers, which could allow for injectable scaffolds. Also many of the natural polymer materials are non-toxic and more or less degradable [80, 81].

Pectin is a natural polysaccharide, which often is used as a gelling agent in the food industry. It is cheap to derive because it exists abundantly in citrus peel and apple pomace, which both are by-products of the juice industry. Pectin is a heteropolysaccharide, meaning that it is composed of galacturonic acid monomers, that occasionally are replaced by rhamnose residues. Pectin is usually classified by the degree of esterification (DE), which is expressed as the percentage of esterified carboxyl groups. High methoxyl pectins (DE > 50%) require high concentrations of soluble solids (sugars) and low pH in order to gel. Low methoxyl pectins (DE < 50%) form gels by addition of calcium or other divalent ions, which allows for gels to form at higher pH [82, 83].

Most studies with pectin are done in relation to its use in drug delivery because pectin has some interesting swelling properties that are pH dependent [84]. Liu and colleagues [85] demonstrated that pectin forms a 3D, spongy structure when prepared by solvent casting followed by freeze-drying. The pores

were around 100 μm in diameter and the walls delineating the pores were less than 1 μm thick. In another study by Liu and colleagues [86], pectin/PLGA composite scaffolds, made by solvent casting and salt leeching, were tested for their protein adsorption and proliferative properties. Their results showed that the amount of adsorbed BSA in the pectin/PLGA was 1.5 times of that found on the PLGA reference. Furthermore, the cells proliferated significantly faster on pectin/PLGA scaffolds after 14 days in culture. It should be noted that in terms of absolute numbers, the cell number only doubled after 14 days of culture for the pectin/PLGA scaffold.

1.5 Project Delimitation and Objectives

In the scope of the background information given in the previous sections, the literature review and the initiating problem, namely "How can the cellular machinery be harnessed through the use of substratum micro- or nanotopographies?", some specific objectives for this project can be formulated. The cell model for this study is confined to ASCs, as these show similar differentiation potential as bone marrow derived MSCs, and in addition are easily obtainable adult SCs. Many novel biosurfaces can be engineered through advanced lithographic techniques, but with more advanced techniques, the price-per-scaffold increases tremendously. Therefore, another criterion for scaffold fabrication systems of this project, is ease of fabrication, e.g. through self-assembly. The project will be delimited to three scaffold systems: Plasma etched polystyrene (PePS), honeycomb patterned polylactic acid (PLA honeycomb) and porous pectin scaffolds.

Tissue culture polystyrene (TCPS) is seen as the "golden standard" for regular expansion of cells in tissue engineering. However, few has investigated the effect of nano-scale roughness of the polystyrene surfaces on the cultured cells. Oxygen plasma etching is a simple method for controlling the substratum roughness of TCPS, and therefore serves as a good system for investigating the effect nanoscale roughness on cells in culture.

The PLA honeycomb system is another interesting system, as it has shown to have some effect on cells. However, where focus previously has been on micro-sized pores, this study take the pore size into the nano regime. Additionally, the author has not been able to find any previous studies with SCs and honeycomb surfaces.

Pectin is a natural polymer found abundantly in citrus peel and its monomeric structure resembles that of hyaluronic acid, a natural glycosaminoglycan that is found abundantly in cartilage. Only one study dealing with cell culturing on pectin scaffolds were found despite that the polymer has been in many researches interest for decades.

All of these surfaces will be tested in terms of protein adsorption patterns, adhesion/spreading, proliferation and differentiation.

Primary Objectives:

- Test if specific cellular responses of the ASCs can be triggered by altering extracellular topographies. These responses should be tested in terms of adhesion, morphology, proliferation and gene expression.

Secondary Objectives:

- Produce and characterize oxygen plasma etched surfaces, PLA honeycomb surfaces and pectin surfaces.

- Design a cell culture system that permits the use of PLA honeycomb substratum.

- Find a method to fabricate pectin scaffolds that are suitable for cell culturing and further analysis.

- Evaluate the biocompatibility of the various surfaces based on their protein adsorption properties.

2

Materials and Methods

2.1 Materials

A detailed list of materials, chemicals and equipment can be found in App.(C).

2.2 Preparation of Surfaces

2.2.1 Oxygen plasma etched polystyrene

Tissue culture treated polystyrene plates (Corning costar) were etched with oxygen plasma at a pressure of 100 $mTorr$, RF (13.56 MHz) effect of 300 W, oxygen flow of 40 $sccm$ and process times between 1 and 10 min. The etching was done using a reactive ion etching system, STS RIE 320 PC.

2.2.2 PLA honeycomb

The fabrication of the PLA honeycomb film was done using a solvent casting method, as described by other research groups [73–76]. Briefly, the method utilizes an amphiphilic surfactant to stabilize the formation of water droplets as the solvent evaporates. In the case of low humidity, no water droplets are formed at the surface of the evaporating solvent, and therefore the surfactant (a phospholipid) micelles act as scaffolds for the emerging pores in the film.

PLA (Aldrich) was dissolved in chloroform (Aldrich) in a concentration of 10 mg/ml. DOPE (Avanti Lipids) was added to give a DOPE to PLA ratio of 1%. 0.9 ml of pure PLA or PLA/DOPE solution was casted on a 26 x 76 mm microscopy glass slide (Menzel Gläser) and allowed to air-dry at room conditions. The humidity had great impact on the final pore size of the honeycomb films, and this was at time of production 33% relative humidity. Before further use, slides were washed with 70% ethanol for sterilization and removal of DOPE residuals.

2.2.3 Pectin gels

Pure pectin with crosslinking

Pectin, from citrus peel (Sigma), was dissolved in MilliQ water to a concentration of 40 mg/ml on a hot plate stirrer, after which the mixture was poured into proper sized culture plates. The solutions were degassed for 30 min, cooled for 2 H at 4 $°C$, frozen for 4 H at -20 $°C$ and freeze-dried (Alpha 1-4 LSC, Christ) with a shelf temperature of -30 $°C$ and a chamber pressure of 1.030 $mbar$. The gels were washed with 100 mM $CaCl_2$ (Merck) solution for 30 min. Crosslinking with EDC/NHS (Sigma/Fluka) or succinyl chloride (Sigma) were also tried instead of the calcium crosslinking. After crosslinking, the gels were washed several times with MilliQ water, cooled, frozen and freeze-dried again. Lastly gels were sterilized by washing them thoroughly with 70% ethanol.

Polyelectrolytic gelling with chitosan

A 2% pectin in 0.1 M HCl solution was mixed with a 2% chitosan (Sigma) in 0.1M HCl in three different ratios: 25/75, 50/50 and 75/25. The different solutions were cast in a proper sized culture plate. Some gels were degassed overnight in a vacuum chamber (named E gels), whereas others were freeze-dried (named L gels), which was done by degassing for 30 min, cooling at 4 $°C$ for 2 H, freezing at -20 $°C$ for 4 hours and freeze-drying. The gels were neutralized by putting the gels in tea filterbags and placing these in a MilliQ water bath over 24 H with several water changes.

2.3 Atomic Force Microscopy

In general, samples (glass or polystyrene) were attached to atomic force microscopy (AFM) metal discs (Electron Microscopy Sciences) with epoxy (Loctite). The samples were imaged using a scanning probe microscope model Nanoscope IIIa (Veeco/Digital Instruments) in tapping mode. Silicon cantilevers (AC-160TS, Olympus) with a resonance frequency around 300 kHz, a spring constant of 42 N/m and a tip radius of 10 nm were applied. Scan speed and feedback settings were adjusted individually for each image, but scan frequency was typically between 1-2 Hz.

Substrate elasticity measurements were conducted in fluid contact mode with a Veeco NP-S10 0.12N/m, pyramid shaped, silicon nitride cantilever with a tip half opening angle of 35°. Data was analyzed using the NanoScope or WSxM software [87].

2.4 Scanning Electron Microscopy

Hydrogel samples required an extra step of preparation compared to other samples. Hydrated samples were prepared for scanning electron microscopy (SEM) by cooling, freezing and freeze-drying. Next the samples were further dehydrated in ethanol series (50, 60, 75, 100%) and put in vacuum chamber for a few hours to evaporate remaining ethanol.

Samples were attached to aluminum stubs (Fisher Scientific) using conductive carbon adhesive tabs (Fisher Scientific), after which they were sputter coated (Edwards, model S150B) with gold and imaged using a scanning electron microscope model 1540 XB (Zeiss) with an accelerating voltage between 5-10 kV.

2.5 Electron-dispersive X-ray Spectroscopy

Samples were attached to aluminum stubs (Fisher Scientific) using conductive carbon adhesive tabs (Fisher Scientific), after which they were sputter coated (Edwards, model S150B) with carbon and analyzed using a SEM model 1540 XB (Zeiss) with EBSD/EDS module.

2.6 Cell Culturing

ASCs were harvested from lipowaste taken from the inner thigh of one 42 year old female donor with a BMI of 20.94. Cells were harvested according to the protocol described by Zuk et al [88]. Cells were cultured in regular growth medium consisting of α-MEM + glutamax (Gibco) + 10% fetal bovine serum (Invitrogen). Pennicillin and streptomycin (Invitrogen) were added to a concentration of 1% along with gentamicin (Invitrogen) at 0.5%. Cells were cultured at 37 $°C$ in a 5% CO_2 and humid atmosphere. Medium was changed twice a week and cells were in general only used below passage 5, however for some spreading experiments, cells were used up till passage 10. Cells were passaged by treating them with 0.125% trypsin/EDTA for 5-7 min, after which the trypsin was inactivated by adding fresh medium. Cells were counted and reseeded at the desired density.

Phase contrast images of the culture were taken using an Axio Observer microscope (Zeiss).

2.7 DNA Quantification using PicoGreen

PicoGreen dsDNA quantization kit (Molecular probes) was used together with alamarBlue to test the sensitivity of the kits in relation to cell number. Cells were lysed in a 0.02% SDS

(Sigma) in TE buffer (Sigma) for 15 min on a rocking shaker. A PicoGreen working solution was prepared by dissolving concentrated PicoGreen in TE buffer (1:200). Cell lysate was mixed with equal volume PicoGreen working solution and transferred to a 96-well microtiter plate. The plate was incubated 10 min at room temperature (RT) under mild shaking. Sample fluorescence was measured at 535 nm with excitation at 485 nm on a Victor^2 1420 microplate reader (Wallac).

2.8 Metabolic Activity Quantification using ala-marBlue

alamarBlue (Invitrogen) was used to estimate the number of cells in a culture. The metabolic activity of mitochondria can be used as an estimate for the total number of cells in a culture, and alamarBlue can therefore be used as an indicator for cell viability and proliferation. alamarBlue was added in a volume equal to 10% of total culture volume. Cultures were then incubated 4 hours at 37 $^\circ C$ before aliquots of 100 μl were transferred to a 96-well microtiter plate. Fluorescence was read at 590 nm with excitation at 544 nm using a Victor^2 1420 microplate reader (Wallac).

2.9 Immunofluorescence of Nuclei, Actin and Vinculin

Cells were rinsed twice in S-PBS and fixed in 4% formaldehyde for 15 min at RT. Next cells were permeabilized with a 0.1% Triton X-100 in PBS solution for 15 min. Non-specific interactions were blocked by incubating cells with 1% BSA in PBS for 30 min at 37 $^\circ C$. Primary rabbit anti-vinculin antibodies (Sigma) in a 2% FBS in PBS (FPBS) solution (1:200) were incubated with the cells for 1 H at 37 $^\circ C$. Secondary goat anti-rabbit Cy5 labelled antibodies (Chemicon) in FPBS (1:150) were added and incubated for 1 H at RT and mild shaking. Finally, Hoechst (Molecular Probes) and bodipy 558/568 labelled phalloidin (Molecular Probes) in PBS (1:2000 and 1:150, respectively) were incubated with the cells at RT for 30 min and mild shaking.

High magnification images of vinculin and stress fibers were obtained using an upright fluorescence microscope (BX61, Olympus), whereas actin mosaic images for cytomorphometry were obtained using an epifluorescent microscope (Axio Observer, Zeiss). Image analysis and cytomorphometry were done using ImageJ[1] version 1.40g.

2.10 Immunofluorescence of Fibronectin

Samples were coated with 0.26 $\mu g/ml$ fibronectin for 1 H at RT. Next surfaces were blocked with 1% BSA in PBS (BPBS) for 1 H at RT. Primary mouse anti-fibronectin antibodies (Sigma) in BPBS (1:2000) were incubated with the surfaces for another 1 H at RT. Lastly secondary goat anti-mouse Alexa 488 antibodies (Invitrogen) in BPBS (1:1000) were incubated under mild shaking with the surfaces for 1 H at RT. Images were either obtained using the BX61 (Olympus) or Axio Observer (Zeiss) microscope.

2.11 Indirect ELISA of Fibronectin

Glass, PLA and PLA honeycomb slides were prepared by outlining a 0.8 cm^2 area with a hydrophobic polymer pen (Dako). Due to the properties of the hydrophobic polymer, ELISA for these surfaces was carried out at RT and approximately twice the incubation time as listed in the protocol beneath was used.

ELISA of fibronectin was carried out by coating samples with either bovine fibronectin (Sigma) or 10% FBS (Invitrogen) for 10 min at 37 $^\circ C$. Washing in between the various steps was done using a 0.05% Tween20 in PBS solution. Blocking of the surfaces was done by incubating with 1% BSA in PBS for 1.5 H at 37 $^\circ C$. Next the surfaces were incubated with mouse monoclonal anti-fibronectin antibodies (Sigma) in BPBS (1:2000) for 1.5 H at 37 $^\circ C$.

---

[1]Freely accessible from http://rsbweb.nih.gov/ij/

Secondary antibodies were horseradish peroxidase (HRP) labeled rabbit polyclonal anti-mouse (DAKO) in BPBS (1:2000), which were incubated for 1 H at 37 $^\circ C$. ELISA substrate solution was prepared by dissolving 4 OPD tablets (DAKO) in 12 ml deionized water mixed with 5 μl 30% perhydrol (Merck). The reaction was carried out at 37 $^\circ C$, and typically stopped after 30 min using a 0.5 M sulfuric acid (Bie&Berntsen) stop solution.

100 μl aliquots of converted substrate were transferred to a 96-well microtiter plate in duplicates, and absorbance was read at 490 nm on a Victor[2] 1420 microplate reader (Wallac).

2.12   Real-Time Quantitative PCR

Cells were lysed and RNA purified using an Aurum Total RNA purification kit (Bio-Rad). RNA concentration and quality were measured using a NanoDrop spectrophotometer (Thermo Scientific). Purity of RNA was measured by the A260/280 ratio, and values between 1.8 and 2.1 were accepted. A total of 1 μg RNA was used for cDNA synthesis, which was set up using an iScript kit (Bio-Rad) and carried out on a GeneAmp 2400 system (Perkin Elmer). Real-time qPCR was set up according to the standard curve method, and standard curves were accepted for $R^2 > 0.98$. The PCR reaction was carried out on a MyIQ iCycler (Bio-Rad). The various primers can be seen in Tab.(2.1).

Table 2.1:   List of primers for real time PCR. *Abbreviations:* YWHAZ: Tyrosine 3-monooxygenase/tryptophan 5-monooxygenase activation protein, zeta polypeptide, PPIA: Cyclophilin A, GAPDH: Glyceraldehyde-3-phosphate dehydrogenase, NES: Nestin, NGFR: Neural growth factor receptor, MYOD1: Myogenic differentiation factor 1, MYF5: Myogenic factor 5, GATA4: GATA binding protein 4, MEF2C: Myocyte enhancer factor 2C, SOX9: Sex determining region Y-box 9, COL2A1: Collagen II alpha 1, ONN: Osteonectin, RUNX2: Runt related transcription factor 2, PPARG2: Peroxisome proliferation activating receptor gamma 2, FABP4: Fatty acid binding protein 4, VWF: Von willebrand factor, VEGFR2: Vascular endothelial growth factor receptor 2, VCL: Vinculin, RHOA: Ras homolog gene family, member A.

Lineage	Gene	Forward primer (5'-3')	Reverse primer (5'-3')
House	YWHAZ	ACT TTT GGT SCS TTG TGG CTT CAA	CCG CCA GGA CAA ACC AGT AT
House	PPIA	TCC TGG CAT CTT GTC CAT	CCA TCC AAC CAC TCA GTC TTG
House	GAPDH	GAA TCT CCC CTC CTC ACA GTT G	GGC CCC TCC CCT CTT CA
Neuro	NES	TAA GGT GAA AAG GGG TGT GG	CCT ACA GCC TCC ATT CTT GG
Neuro	NGFR	CCC TGT CTA TTG CTC CAT CC	CCT TGC TTG TTC TGC TTG C
Skeletal	MYOD1	AAC GGA CGA CTT CTA TGA CG	AGT GCT CTT CGG GTT TCA GG
Skeletal	MYF5	TGA TTG AGG GTA GCT TGT TGC	CAC CAG AGA CAT TTT GAT GAG C
Cardiac	GATA4	GCC TGG CCT GTC ATC TCA CT	ACA TCG CAC TGA CTG AGA ACG
Cardiac	MEF2C	CCC TGC CTT CTA CTC AAA GC	CGT GTG TTG TGG GTA TCT CG
Cartilage	SOX9	CAC ACA GCT CAC TCG ACC TTG	TTC GGT TAT TTT TAG GAT CAT CTC G
Cartilage	COL2A1	GGC AAT AGC AGG TTC ACG TAC A	CGA TAA CAG TCT TGC CCC ACT T
Bone	ONN	GGC CTG GAT CTT CTT TCT CC	CCT CTG CCA CAG TTT CCT TC
Bone	RUNX2	GGC AGC ACG CTA TTA AAT CC	GTC GCC AAA CAG ATT CAT CC
Adipose	PPARG2	CCA CAG GCC GAG AAG GAG AAG C	GCC AGG GCC CGG AGG AGG TCA G
Adipose	FABP4	ATG GGA TGG AAA ATC AAC CA	GTG GAA GTG ACG CCT TTC AT
Endothelial	VWF	CGG CTT GCA CCATT CAG C	GAT GAG ACG CTC CAG GAT GG
Endothelial	VEGFR2	CAG GAT GGC AAA GAC TAC ATT G	GAG GAT TCT GGA CTC TCT CTG CC
Adhesion	VCL	GGG CAG TGT TTC CTT TTT GG	TCA TCT GGT TCT GGC TTT GG
Signaling	RHOA	GCA GGT AGA GTT GGC TTT GTG G	CTT GTG TGC TCA TCA TT

2.13   Statistics

Statistical analysis was performed using SPSS version 17. Data is represented as mean $\pm$ standard error of mean (SEM) unless otherwise stated.

Large datasets were evaluated for normality using Q-Q plots and the Kolmogorov-Smirnov test, whereas normality was assumed for small datasets. Datasets with non-normal distributions were evaluated with non-parametric tests. Levene's test was used to address equality of sample variance. For normal distributed data, Student's t-test was applied for comparison of means, whereas one-way ANOVA combined with Tukey HSD post hoc tests were applied for multiple sample comparisons. The non-parametric equivalents were the Mann-Whitney U and Kruskal-Wallis tests, respectively. The level of significance was set to $p < 0.05$.

3

Results

Many different experiments have been conducted in relation to this project, so to ease the reading and interpretation, the results are divided into three groups representing the different culturing systems. Furthermore, some preliminary experiments have been conducted, and these are assembled in one section.

3.1 Preliminary Experiments

3.1.1 alamarBlue versus PicoGreen

This experiment was conducted in order to evaluate the validity and reliability of alamarBlue in terms of quantifying proliferation of cells. DNA quantification, using PicoGreen dsDNA quantification kit, was set as the reference for the experiment, as PicoGreen is well-known for its high sensitivity and reliability [89]. Additionally, this experiment was set up in order to find the proper incubation time for alamarBlue with ASCs.

For the alamarBlue, ASCP6 cells were seeded in different quantities (4000-62.5) in duplicates in a 96-well microtiter plate (Corning costar). alamarBlue was added in a volume equal to 10% of the culture volume and measurements of the plate were obtained every hour for the initial 6 hours of incubation and again after 21 hours. For PicoGreen, ASCP6 cells were serially diluted (20,000-78.125 cells) in eppendorf tubes, after which the amount of DNA was probed according to the protocol described in Sec.(2.7).

The different standard curves with fitted line are plotted in Fig.(3.1), where (A) represents the PicoGreen standard curve, (B) and (C) represents the alamarBlue standard curves from 0-6 hours incubation and at 21 hours, respectively. Furthermore, the coefficients of determination (R^2) are listed in Tab.(3.1).

The results demonstrate that alamarBlue can be utilized as probe for quantifying proliferation of cells in culture. Although the coefficients of determination were slightly lower than that for the PicoGreen standard, they were still within the acceptable range if incubation periods of 3-5 hours were chosen.

Furthermore, it should be noted that another standard curve with fluorescence as function of cell number was made by serially diluting a known cell stock (data not shown). This was done in order to test if subsequent prolifera-
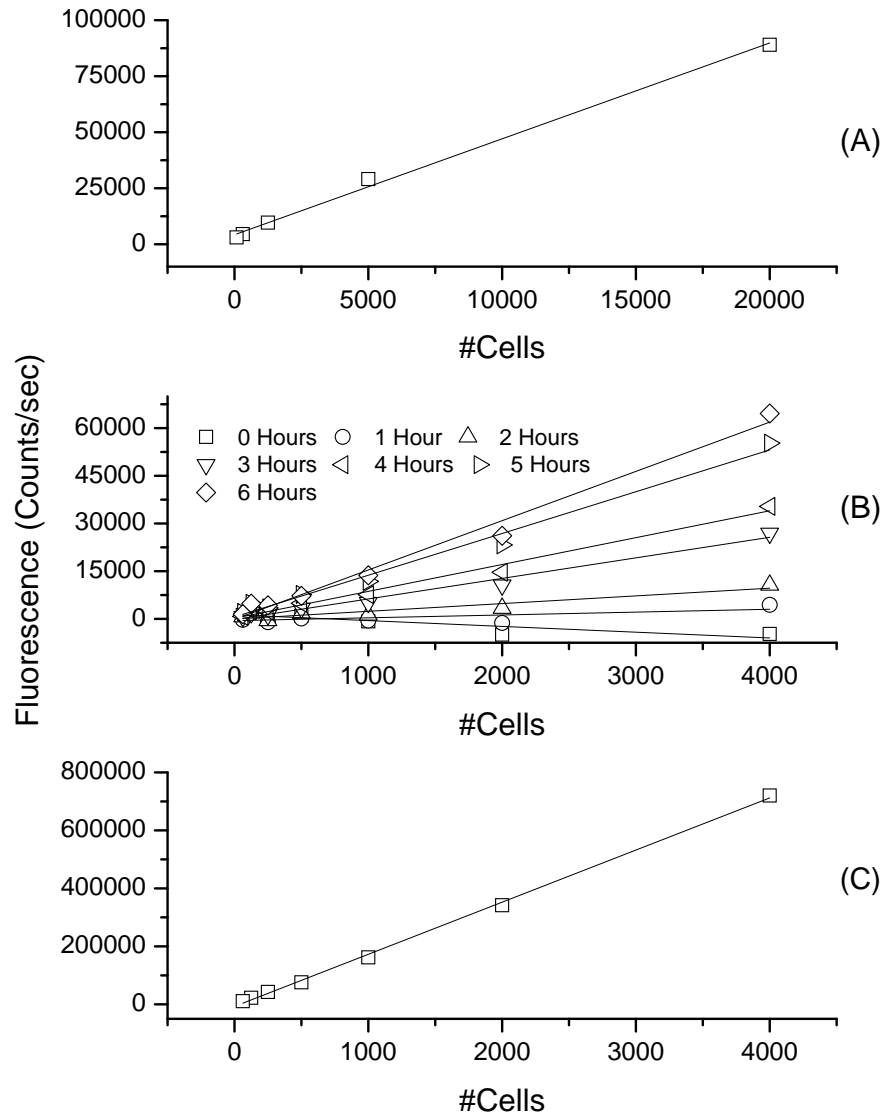
Figure 3.1: **Cell quantification standard curves**. (A) shows the curve for PicoGreen, (B) alamarBlue 0-6 hours and (C) alamarBlue after 21 hours.

tion results could be presented as: "Total cells as function of time" instead of "fluorescence as function of time". First indication was positive, as the data correlated linearly with an R^2-value of 0.985, however when using this "fluorescence to number of cells" conversion factor at near-confluent cells, it resulted

Sample	R^2		Sample	R^2
PicoGreen	0.99592		AB 4H	0.98370
AB 0H	0.28488		AB 5H	0.98303
AB 1H	0.86862		AB 6H	0.73028
AB 2H	0.97872		AB 21H	0.99861
AB 3H	0.98510			

Table 3.1: Coefficients of determination for the fitted lines in Fig.(3.1).

in a cell density of almost 70,000 $cells/cm^2$, which is more than 2.5 times the density of manually counted cells at 95-100% confluency. For this reason, the subsequent proliferation data is presented as fluorescence as function of time.

3.2 Oxygen Plasma Etched Polystyrene Surfaces

3.2.1 Topographical Analysis of PePS Surfaces

The topography of plasma etched polystyrene (PePS) surfaces was examined by attaching TCPS pieces to AFM metal wafers and etching the TCPS using various process times (0-10 min). Fig.(3.2) shows the results of the analysis, where (A-C) and (D-F) show the topographies and profiles (along the green line) for the 0 min, 5 min and 10 min samples, respectively. These indicate that process time greatly influenced the topography of the samples. The RMS, average (R_a) and peak-valley (R_{TM}) roughness of the surfaces increased significantly when process time was prolonged as illustrated seen in Tab.(3.2). Furthermore, the percent-wise increase in effective surface area, which was calculated using the AFMSurfaceArea.m script found in App.(A), can be seen in the table as well. This surface area also followed the trend of the RMS roughness, and showed up to $92 \pm 29\%$ increase after $10min$ of etching.

Table 3.2: Roughness parameters for the oxygen plasma etched surfaces. *Statistics:* Data is represented as mean $\pm$ SEM, *: $p \leq 0.05$, **: $p \leq 0.01$, ***: $p \leq 0.001$ compared to TCPS using Student's t-test (n=3).

Sample	$\mathbf{R}_a$ [nm]	$\mathbf{R}_{RMS}$ [nm]	$\mathbf{R}_{TM}$ [nm]	$\mathbf{A}_{Eff}$ [%Increase]
TCPS	4.01 $\pm$ 0.30	5.27 $\pm$ 0.36	29.36 $\pm$ 5.12	0.52 $\pm$ 0.13
PePS1	4.33 $\pm$ 0.16	5.75 $\pm$ 0.26	39.99 $\pm$ 7.13	1.23 $\pm$ 0.04 (*)
PePS3	8.27 $\pm$ 0.65 (*)	10.88 $\pm$ 0.87 (*)	90.00 $\pm$ 11.07 (*)	8.35 $\pm$ 1.31 (*)
PePS5	18.45 $\pm$ 0.44 (***)	24.01 $\pm$ 0.58 (***)	115.89 $\pm$ 9.24 (**)	32.33 $\pm$ 1.55 (***)
PePS7	36.58 $\pm$ 1.98 (**)	48.00 $\pm$ 2.69 (**)	141.13 $\pm$ 7.98 (***)	55.92 $\pm$ 1.19 (***)
PePS10	55.02 $\pm$ 9.51 (**)	71.87 $\pm$ 13.60 (**)	353.75 $\pm$ 173.04	91.75 $\pm$ 29.32

It should be noted that a 20 min was prepared as well, however oxygen plasma etching for 20 min resulted in severely deformed polystyrene wafers, and thus 10 min was set as the cutoff for the processing time range.

The SEM of the RMS roughness and the effective area demonstrate that surface topography can be controlled fairly good with process times up to 7 min.

In order to minimize the number of samples for the biological assays, 5, 7 and 10 min, as well as the TCPS reference, were used for further experiments.

3.2.2 Analysis of Elemental Composition of PePS Surfaces

Due to the volatile nature of the etching process with oxygen plasma, it is likely that the etching, in addition to altering topography, incorporates oxygen into the surface of the samples. To test this, samples were etched as described in Sec.(2.2.1) and prepared for electron-dispersive x-ray spectroscopy (EDS) according to the method described in Sec.(2.5). EDS is a technique that measures the x-ray back scatter from a sample when bombarding it with high energy electrons. Briefly, the electrons may excite an electron from an inner shell of an atom, which then is occupied by an electron coming from an outer shell. The difference in energy levels between the shells is released in form of x-ray, which can be picked up by the analyzer. The counts and energy distribution gives the researcher an idea of the elemental composition of the sample.

Fig.(3.3) shows count versus energy plots, that for all samples have been normalized to the carbon peak. It shows that for TCPS, PePS5 and PePS7,
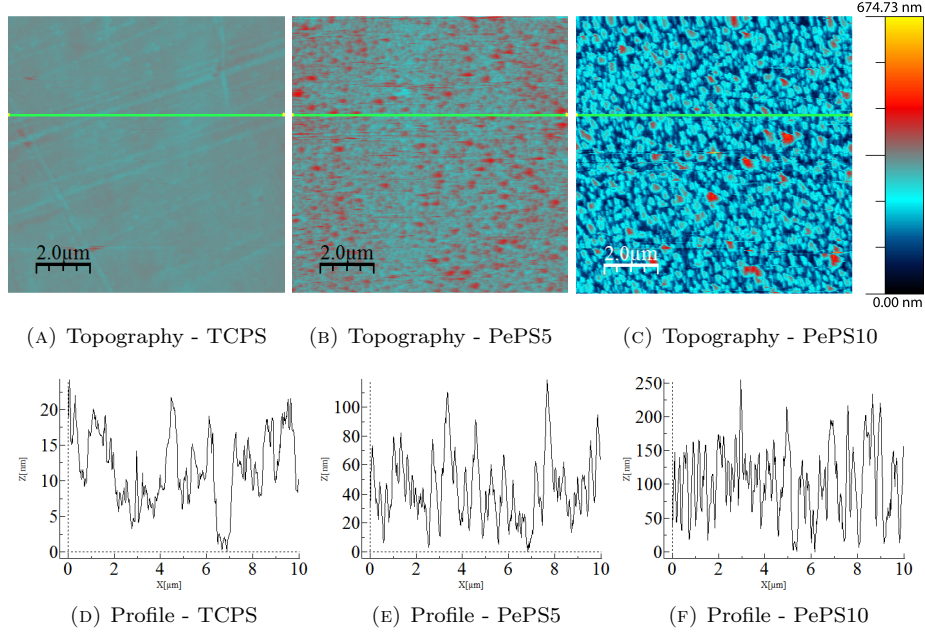
(A) Topography - TCPS   (B) Topography - PePS5   (C) Topography - PePS10

(D) Profile - TCPS   (E) Profile - PePS5   (F) Profile - PePS10

Figure 3.2: **Roughness of plasma-etched TCPS.** (A-C) show the topography of the 0 min, 5 min and 10 min samples, respectively. (D-F) show the profiles along the green lines.

there was a gradual increase in the amount of oxygen in the surfaces. The PePS10 sample does not follow the trend, however it should be noted that this sample had a significantly different surface topography, which probably was due to re-polymerization after the sample might have reached its glass transition temperature. This was also confirmed by visual inspection, as the polystyrene partly had lost its transparency.
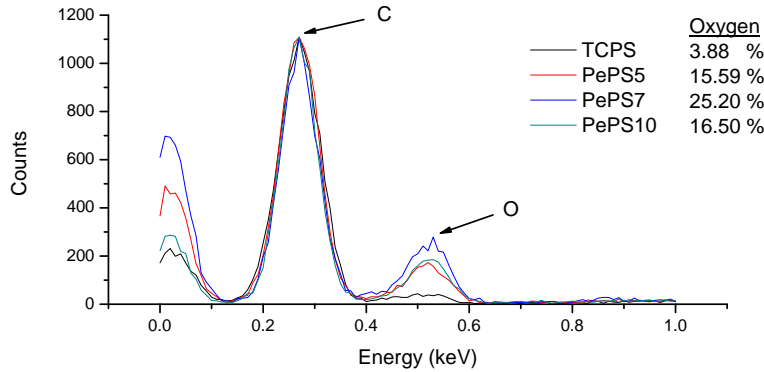

Figure 3.3: **Elemental composition of the plasma etched polystyrene.** Oxygen concentration is shown for the various samples. The graphs have been normalized to the carbon peak.

3.2.3 Fibronectin Adsorption to PePS Surfaces

The effective surface area of polystyrene increased significantly when exposed to oxygen plasma etching, and this might effect the protein adsorption properties. To evaluate this, etched polystyrene was examined in terms of fibronectin adsorption. This was done by using an indirect ELISA setup according to the method described in Sec.(2.11).

Two protein coatings were used, one consisting of fibronectin alone and another of 10% FBS, which is a complex mixture of different proteins. The results in Fig.(3.4) indicate that protein adsorption dynamics changed tremendously when surfaces were exposed to oxygen plasma etching. For the pure fibronectin solution coating, a large reduction in protein adsorption was observed on the etched plates compared to TCPS. However, for the FBS coating an interesting adsorption pattern emerged. Here the amount of adsorbed fibronectin increased with increasing roughness. This contradictory result might indicate that protein adsorption kinetics is not as straightforward as first hypothesized, and that the complex mixture of proteins in FBS might help facilitate adsorption of fibronectin.
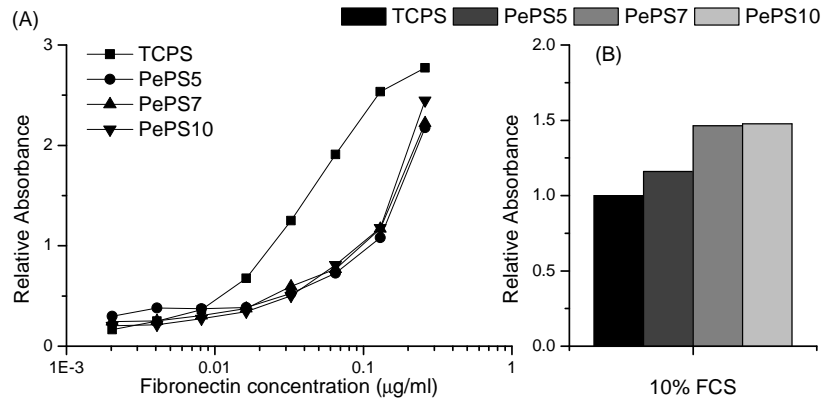

Figure 3.4: **Fibronectin Adsorption to plasma etched polystyrene.** (A) shows ELISA substrate absorbance as function of coating concentration of pure bovine fibronectin, whereas (B) shows the substrate absorbance after 10 min of incubation with 10% FBS.

3.2.4 Spreading of Cells on PePS Surfaces

The spreading of ASCs were characterized by phase contrast microscopy by seeding ASCP9 cells at $1500/cm^2$ and obtaining phase contrast images after 24, 48 and 96 hours. The results in Fig.(3.5) reveal that no significant difference in spreading dynamics was observed between the four samples. Already after 24 hours, cells showed good spreading, and after 48 hours all cells were completely spread. From a proliferation point-of-view, there might be a slight increase in cell numbers with increasing roughness.

To better quantify the morphology of the cells, a cytomorphometry experiment was conducted by seeding ASCP6 at $1500/cm^2$ for 48 hours before cells were fixed and stained for actin and nuclei according to protocol in Sec.(2.9).

5x5 mosaic images were obtained and analyzed. The images in Fig.(3.6A-D) reveal no obvious difference between the samples. However, morphometry analysis reveal, that the etched surfaces differed from the TCPS reference in terms of cell circularity, major axis, minor axis, elongation and perimeter. The results furthermore indicate that the cells on the PePS10 surface had slightly different morphology than cells on PePS5 and 7. This is not only observed through significant difference in circularity, but also indirectly through the non-significant differences of the other parameters.

The actin and vinculin distribution in the cells was examined by culturing ASCP5 at 1500 cells/cm^2 for 3 days, after which cells were fixed and stained according to method described in Sec.(2.9). The results in Fig.(3.7) clearly demonstrate that all cells formed stress fibers and had punctual focal adhesion spots. Looking at the actin distribution, it appears that the orientation of the stress fiber formation became more uniaxial as the roughness of the surface increased. Furthermore, the size of the individual focal adhesion spots seemed to decrease with increasing roughness.

Conjointly, these spreading results indicate that cells respond differently to the etched nanorough surfaces compared to the TCPS reference, and that there might be an effect of increased etching process time.
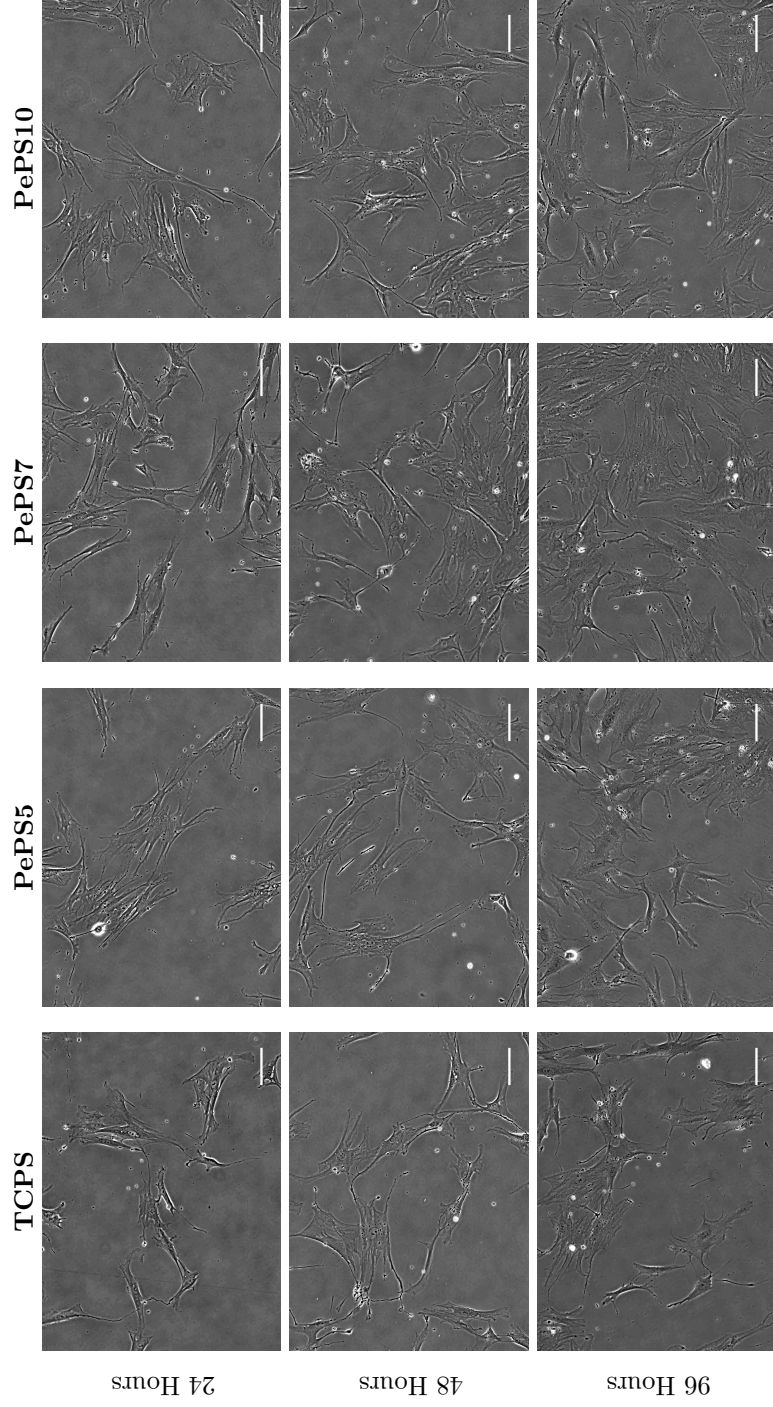
Figure 3.5: **Spreading dynamics of cells cultured on plasma etched polystyrene surfaces.** Phase contrast microscopy images were obtained at 10x magnification after 24, 48 and 96 hours of culturing. The scale bar represents 100 μm.
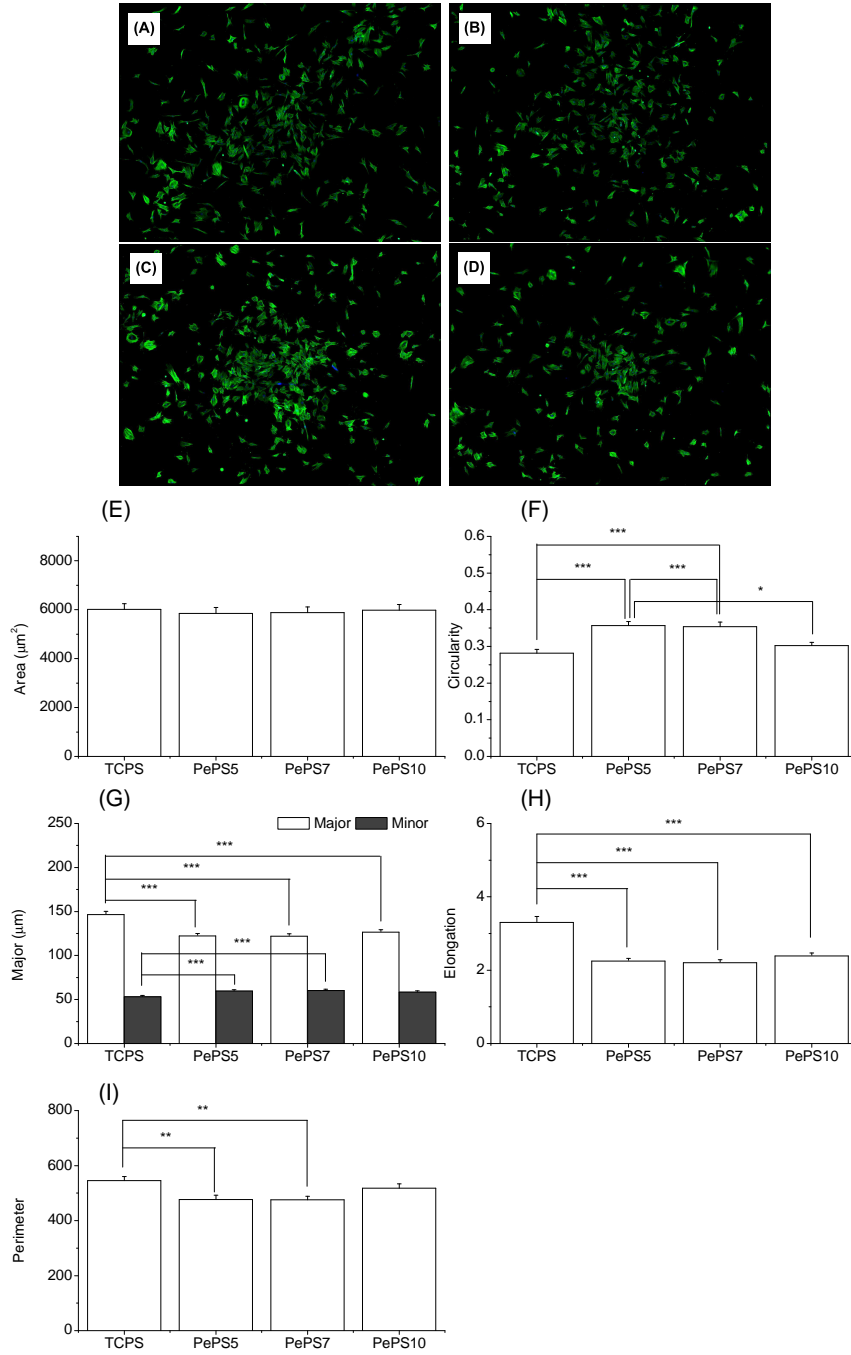
Figure 3.6: **Cytomorphometry of cells cultured on plasma etched polystyrene surfaces.** Immunofluorescence images were obtained after 48 hours of culturing. (A-D) show 5x5 mosaic images of the actin/nuclei stained cells on the various surfaces. Cell morphology was characterized in terms of area (E), circularity (F), major and minor axis of fitted ellipse (G), elongation (H) and perimeter (I). *Statistics:* mean $\pm$ SEM. *:$p \leq 0.05$, **:$p \leq 0.01$, ***:$p \leq 0.001$ using ANOVA and Tukey HSD post hoc test (n$\approx$150).

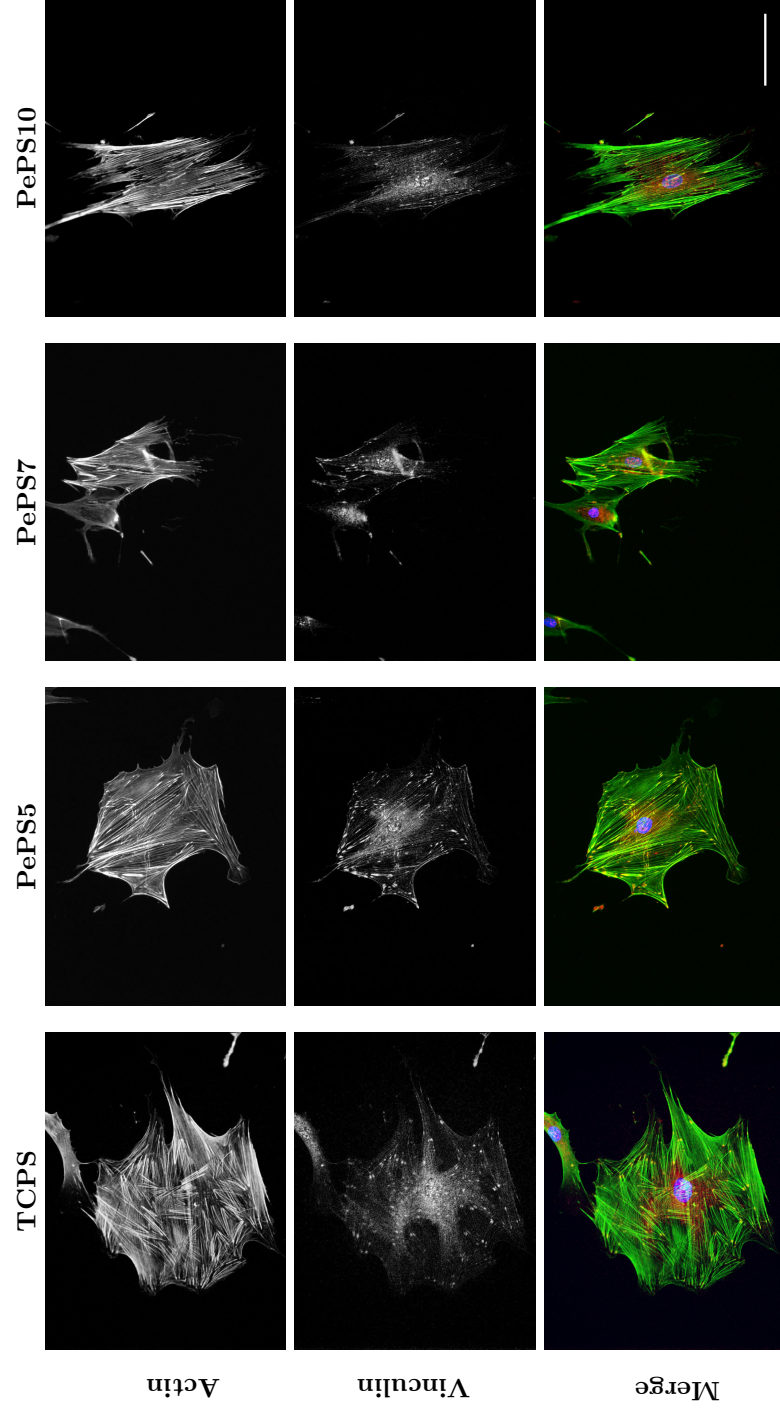Figure 3.7: **Vinculin and stress fiber distribution in cells cultured on plasma etched polystyrene.** Immunofluorescence images were obtained at 20x magnification after 72 hours of culturing. Top row shows actin distribution, mid row shows vinculin distribution and bottom row shows the merge of actin, vinculin and nuclei. The scale bar represents 100 μm.

3.2.5 Proliferation of Cells on PePS Surfaces

To evaluate the proliferative properties of the oxygen etched plasma surfaces, a proliferation experiment with alamarBlue was conducted. ASCP4 cells were seeded in quadruplicates at 1500 per cm^2 and cultured for 9 days with medium change every second day. The metabolic activity was measured every day using alamarBlue. The results are presented in Fig.(3.8) as average fluorescence intensity per sample as function of time as well as the calculated doubling times.

The results show a slight difference between the samples with the 10 min sample showing the highest proliferation from day 5 to 9. However, based on the doubling times obtained from the two independent experiments, there was no significant difference between the surfaces using ANOVA statistics.
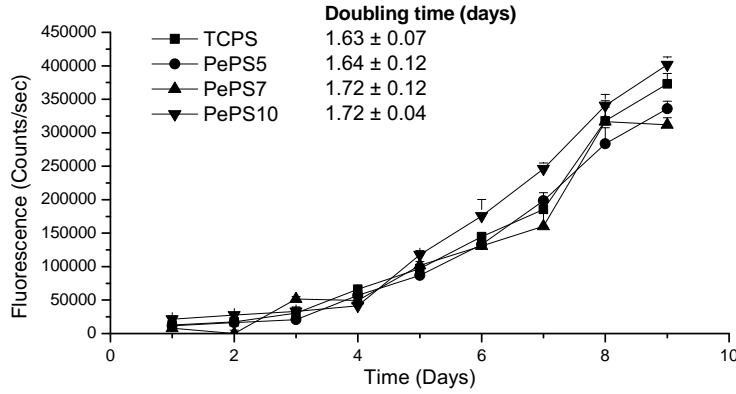

Figure 3.8: **Proliferation of cells cultured on polystyrene.** data is represented as mean fluorescence ± SEM as function of time. The doubling times are presented as mean ± SEM in days.

3.2.6 Transcriptional Analysis of Gene Expression of Cells on PePS Surfaces

The expression of some lineage and adhesion related genes were evaluated for cells on the various nanorough surfaces. ASCP2 cells were seeded at 5000 per cm^2 and cultured for 14 days in regular growth medium. The cells were lysed, RNA purified and analyzed according to the method described in Sec.(2.12).

The results shown in Fig.(3.9) was normalized to the TCPS reference to ease the comparison between the samples. (A) shows the housekeeping gene level as well as the calculated geometric mean (in absolute expression), which, apart from the TCPS reference, was fairly stable among the samples. The stability of absolute housekeeping gene expression reflects the precision in the RNA concentration measurements. Regarding neural, skeletal muscle, cardiac muscle, adipose tissue and endothelial genes, sample levels were so low compared to the positives, that the intersample difference is without any biological significance. MEF2C and PPARG2 showed decent sample levels and small upregulations for the samples compared to TCPS. However, as GATA4 and FABP4 showed no or little expression compared to the positive control, it is questionable whether the MEF2C and PPARG2 regulations were related to differentiation of cells.

As for cartilage related genes, there might be a small upregulation in COL2A1 peaking at 3-fold upregulation at PePS7 and 10 samples. Likewise, RUNX2, a transcription factor involved in osteogenesis, appears to be upregulated for increasing substrate roughness. However, the appertaining positive control does show the anticipated high levels of expression for RUNX2 and ONN. This obscures the meaning of the differences found between the samples.

Vinculin expression in the cells also showed a small, but gradual, increase as substrate roughness increased. Lastly RhoA, an intracellular signaling molecule, was greatly upregulated for cells cultured on the rougher PePS7 and PePS10 surfaces.
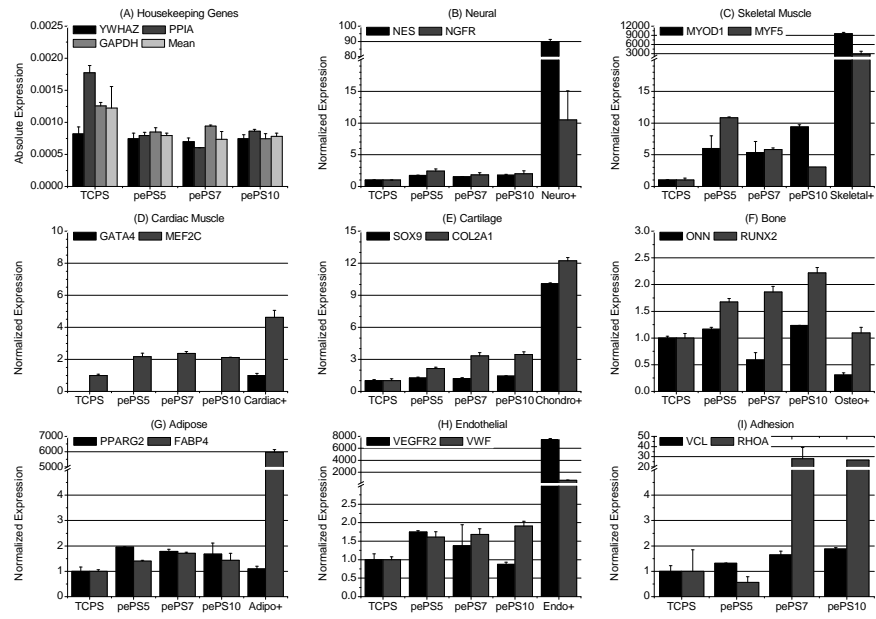
Figure 3.9: **Transcriptional analysis of gene expression of cells cultured on PePS surfaces.** Data is presented as mean ± SEM. (A) shows the absolute expression levels of the housekeeping genes as well as the geometric mean. (B-H) show the lineage specific expression and (I) shows the adhesion related expression levels - all normalized to housekeeping gene and polystyrene reference. GATA4 expression is normalized to positive due to being 0 for all other samples.

3.3 Honeycomb Polylactic Acid Surfaces

3.3.1 Topographical and Structural Analysis of PLA Honeycomb Surfaces

PLA honeycomb surfaces were prepared as described in Sec.(2.2.2) and examined using AFM and SEM - see Fig.(3.10). The AFM image of the surface reveals that 15.5% of the surface was covered with nanosized pores with an average diameter of 322 ± 0.004 nm. The appertaining profile reveals that the pores were about 50 nm deep. However, judging from the parabolic shape of the profile curve, it appears that the pores in fact were deeper and that the current profile was a result of repulsive electrostatic interaction between the sample and the AFM tip. The SEM images revealed that the pores covered the surface in a uniform distribution. Furthermore, the images confirmed the pore size measurements obtained by AFM. It should be noted that the cracks seen in the 12,000x magnification SEM image are not inherent artifacts, but simple damage due to adsorption of energy from the accelerated scanning electrons.

3.3.2 Fibronectin Adsorption to PLA Honeycomb Surfaces

The protein adsorption to the surfaces was examined using an indirect ELISA setup as described in Sec.(2.11). The surfaces were coated with a 0.26 $\mu g/ml$ fibronectin solution as well as a 10% FBS solution. The results of the analysis are shown in Fig.(3.11) and demonstrate that the TCPS surface had significantly higher protein adsorption compared to glass, PLA and PLA honeycomb - both for pure fibronectin as well as 10% FBS coating. Furthermore, the results indicate a significantly higher adsorption to PLA honeycomb compared to the flat PLA films and the glass. This could explained by interaction of the proteins with the nanopores of the PLA honeycomb film.

To investigate this, an immunofluorescence staining was performed of the fibronectin coated PLA honeycomb surface according to the protocol in Sec.(2.10). The images in Fig.(3.12) were obtained using a high numerical aperture, 63x water immersion objective. From the images it is evident that protein adsorption occurred in some sort of pattern, and not in a uniform layer as with TCPS and flat PLA (data not shown). The blow-up reveals that the signal came from localized dots corresponding to pores with a width of 432 ± 0.010 nm.

3.3.3 Spreading of Cells on PLA Honeycomb Surfaces

Spreading of cells cultured on PLA honeycomb were addressed using phase contrast images, cytomorphometry of actin stained cells and images of stress fiber and vinculin distribution.

For phase contrast microscopy, ASCP7 cells were seeded at 1500 per cm^2 and cultured for 4 days. Phase contrast images were obtained after 24, 48 and 96 hours to follow the spreading dynamics of the cells. The results in Fig.(3.13) show that already after 24 hours, the morphology of cells cultured on PLA and PLA honeycomb differed from that of cells cultured on TCPS and glass. Cells on TCPS and glass spread more to cover a larger area and were in general not very elongated. On the contrary, cells on PLA and PLA honeycomb had much
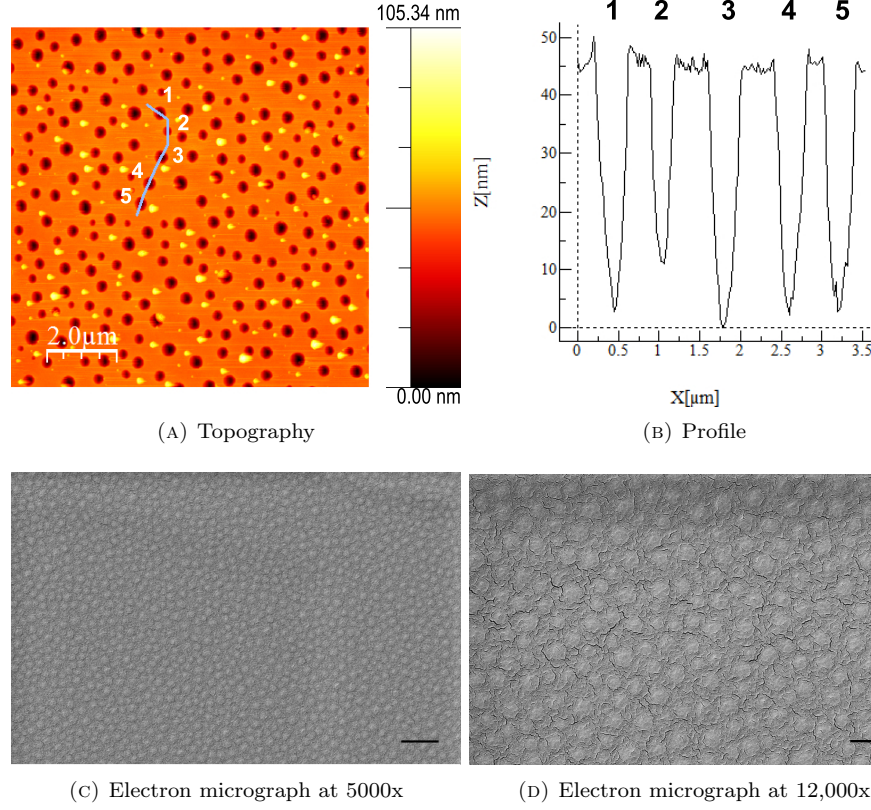
(A) Topography

(B) Profile

(C) Electron micrograph at 5000x

(D) Electron micrograph at 12,000x

Figure 3.10: **Topography and Structure of PLA Honeycomb surfaces.**
(A) Shows the topography of the surfaces after DOPE micelles have been washed
off the surface. (B) shows the profile along the blue line of the AFM image in (A).
(C) and (D) show electron micrographs of the honeycomb structure (including
DOPE micelles) at 5000x (scale bar represents 5 μm) and 12,000x (scale bar
represents 1 μm) magnification, respectively.

narrower cell bodies and elicited a more elongated phenotype. This difference
in spreading only became more prominent after 48 and 96 hours.

To quantify the morphology, cytomorphometry of actin stained cells were
conducted. ASCP4 cells were seeded at 1500 per cm^2 and cultured for 4 days be-
fore they were fixed and stained according to the method described in Sec.(2.9).
3x3 mosaic images were obtained at 10x magnification using the Axio Observer
(Zeiss) microscope and analyzed based on cell area, circularity, ellipse fitting
(major and minor axis), elongation and perimeter. The results in Fig.(3.14)
both indicate some direct statistical differences between the samples, and some
indirect, but non-significant, differences between PLA and PLA honeycomb.
First, there was a significant difference between glass and PLA in terms of cir-
cularity and minor axis. Second, there was a significant difference between glass
and PLA honeycomb in terms of area, minor axis and elongation. Third, there
was a significant difference between PLA and PLA honeycomb in terms of circu-
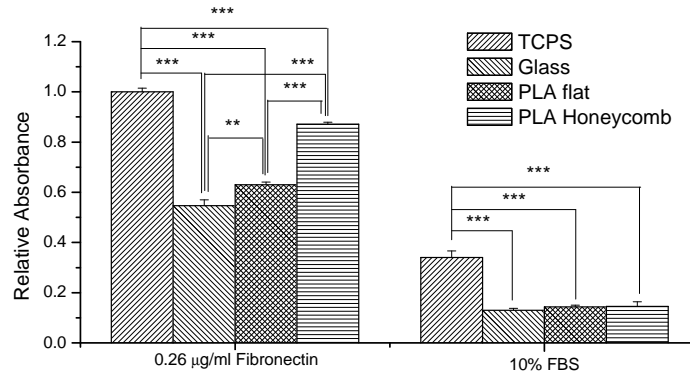
Figure 3.11: **Fibronectin adsorption to PLA Honeycomb.** Shows normalized ELISA substrate absorbance using both pure fibronectin and 10% FBS as coating. *Statistics:* Mean ± SEM (n=2). **: $p \leq 0.01$, ***: $p \leq 0.001$ using ANOVA and Tukey HSD post hoc test. *: Relative to TCPS. #: Relative to PLA.

(A) Original   (B) Blowup of selection
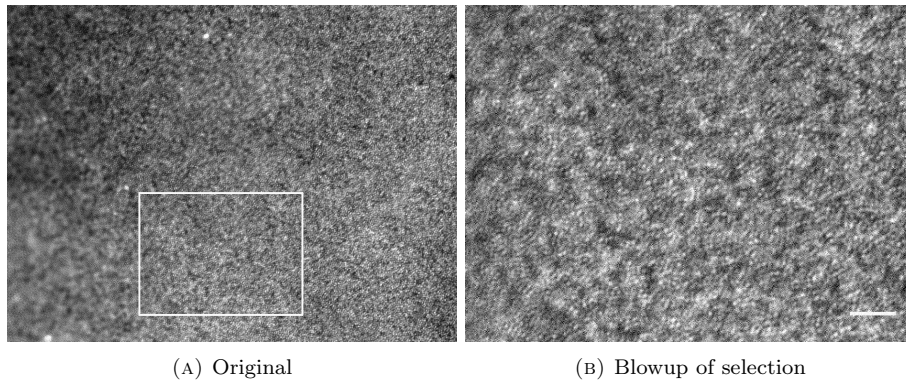
Figure 3.12: **Immunofluorescence of protein adsorption to PLA Honeycomb.** (A) is obtained using a 63x/1.2 W NA/water immersion objective. (B) shows a blowup of the selection showed in image (A). Scale bar represents 5 μm.

larity and perimeter. Fourth, conjoining these differences, one could hypothesize that there was a difference in area and elongation of cells cultured on PLA and PLA honeycomb, however due to the sample size, it was not statistically proven.

The elongation of cells could influence the distribution of intracellular focal adhesions. To evaluate this, ASCP4 cells were seeded on the various surfaces at 1500 cells per cm^2 and cultured for 4 days before stained according to the method described in Sec.(2.9). The results here indicate that elongated cells, which were found at a higher frequency on PLA and PLA honeycomb surfaces, had fewer and less localized focal adhesions compared to the well spread cells on e.g. glass, see Fig.(3.15). The cells on the PLA and PLA honeycomb were furthermore characterized by a clearly defined leading edge and tail, which could
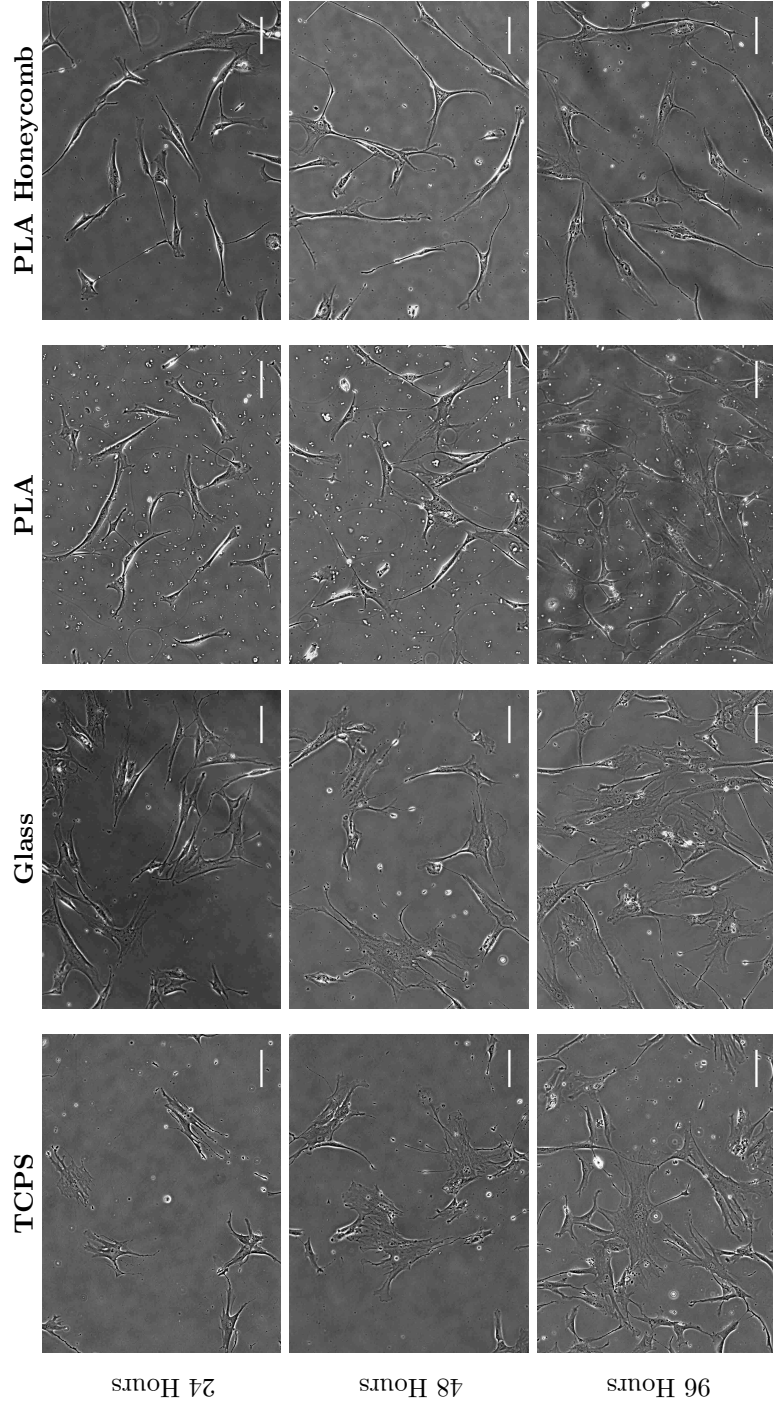
Figure 3.13: **Spreading dynamics of cells cultured on PLA Honeycomb.** Phase contrast microscopy images were obtained at 10x magnification after 24, 48 and 96 hours of culturing. The scale bar represents 100 μm.

indicate a high level of migration on these surfaces. This also coheres with the low amount of stress fibers found in these cells, as migrating cells might not have the time to organize and develop a large stress fiber network.

(A) Glass　　　　　(B) PLA　　　　　(C) PLA Honeycomb
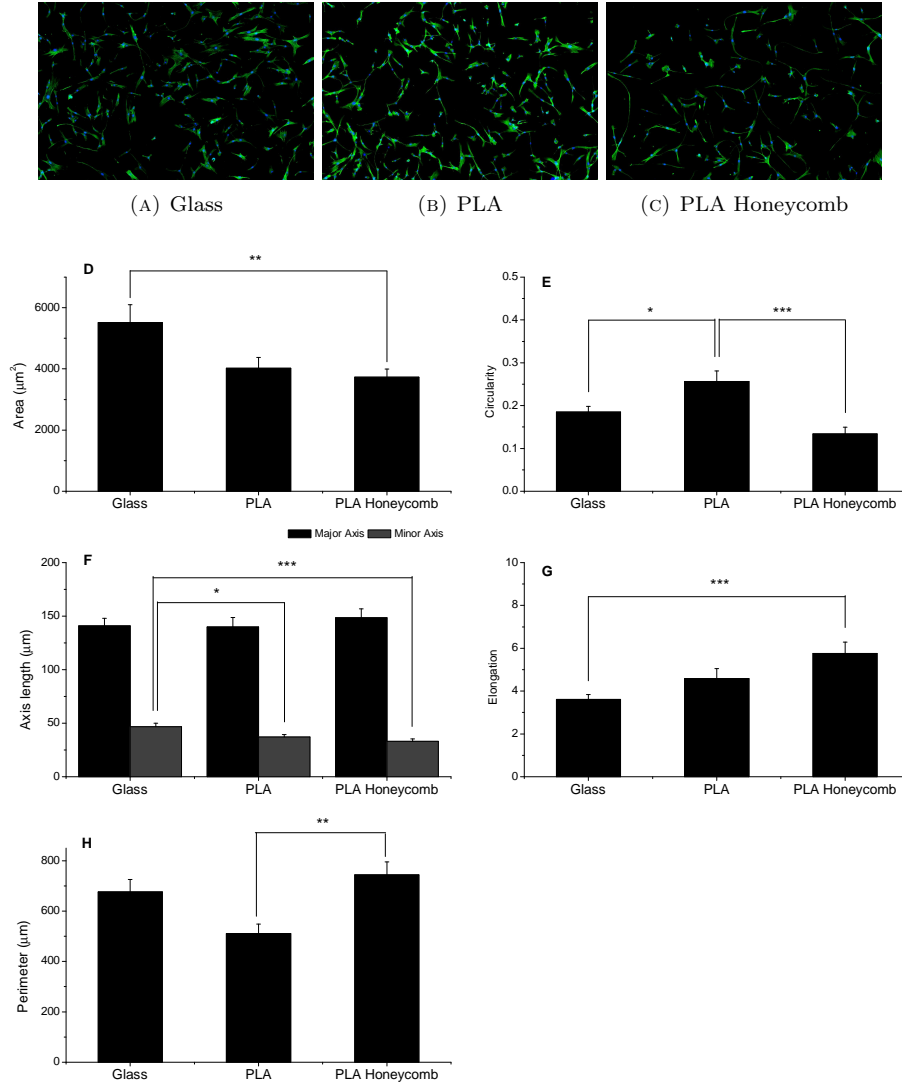
Figure 3.14: **Immunofluorescence imaging of cells cultured on PLA Honeycomb.** (A-C) show 3x3 mosaic images obtained at 10x magnification of cells cultured on glass, PLA and PLA Honeycomb, respectively. (D-H) shows the spreading statistics based on cell area, circularity, elongation (major-to-minor axis ratio) and perimeter. *Statistics:* Data is represented as mean $\pm$ SEM. *:$p \leq 0.05$, **:$p \leq 0.01$, ***:$p \leq 0.001$ using ANOVA and Tukey HSD post hoc test (n$\approx$60).
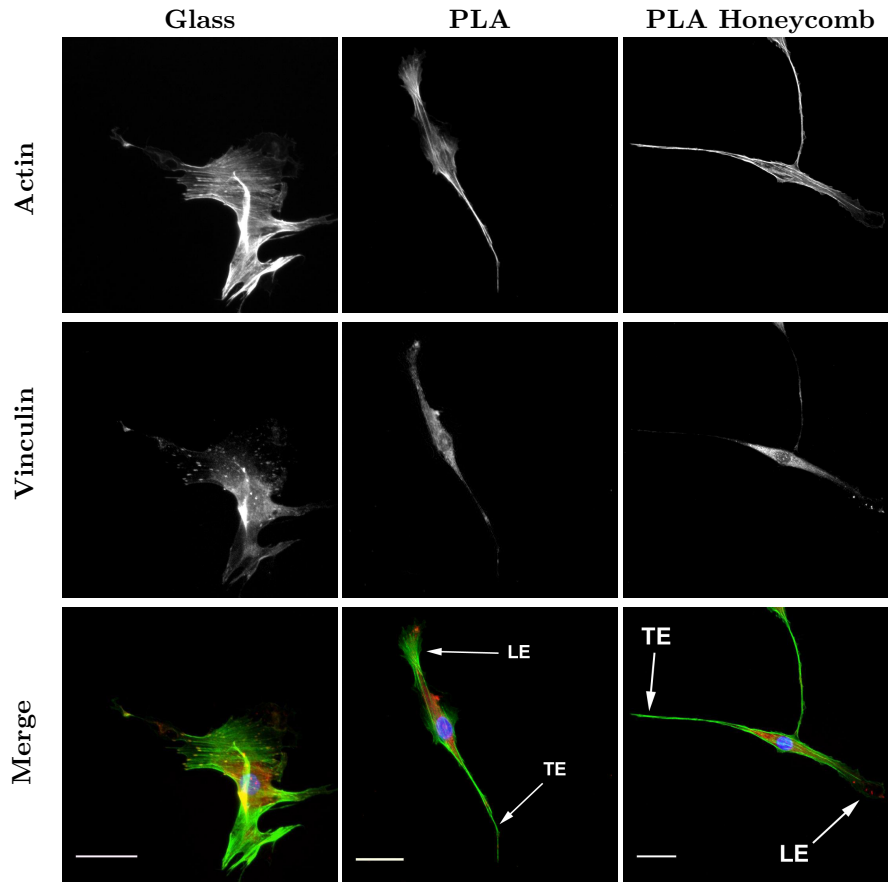
Figure 3.15: **Actin and vinculin distribution in cells cultured on PLA Honeycomb.** Images were obtained at 20x magnification and scale bars represent 50 μm. The arrows indicate the leading edge (LE) and trailing edge (TE).

3.3.4   Proliferation of Cells on PLA Honeycomb Surfaces

The proliferative properties of the PLA honeycomb films were evaluated using the alamarBlue assay and compared to TCPS, glass and flat PLA references. ASCP4 cells were seeded at 1500 per cm^2 and cultured for 10 days. The metabolic activity was evaluated every second day using alamarBlue according to the method described in Sec.(2.8).

The results indicate a clear difference in the proliferative properties, as TCPS and glass showed higher proliferation compared to the PLA's from start to end. Based on the day 6, 8 and 10 measurements, the results show that cells proliferated significantly faster on the TCPS and glass surfaces compared to the flat PLA or honeycomb PLA. No differences were observed between flat PLA and PLA honeycomb surfaces.
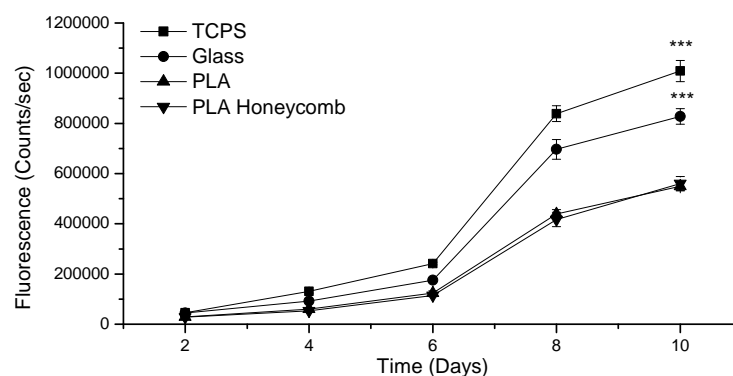
Figure 3.16: **Proliferation of cells cultured on PLA Honeycomb.** The data is represented as mean fluorescence $\pm$ SEM (n=6) as function of time. *Statistics:* Based on day 6, 8 and 10 measurements. ***, $p \leq 0.001$ using ANOVA and Tukey HSD post hoc test.

3.3.5   Transcriptional Analysis of Gene Expression of Cells on PLA Honeycomb Surfaces

The spontaneous differentiation of cells were probed using real-time qPCR. ASCP2 cells were seeded at 5000 per cm^2 and cultured for 14 days in regular growth medium before they were lysed, and RNA was purified and analyzed as described in Sec.(2.12).

The results in Fig.(3.17) show the relative expression of several lineage and adhesion related genes. YWHAZ, PPIA and GAPDH were selected as housekeeping genes as shown in (A). The other charts demonstrate that no significant differences were observed between the glass, PLA and PLA honeycomb. If any expression difference between the surfaces occurred, it was insignificant in relation to the positive control.

As with the gene expression results of the plasma etched surfaces (see Sec.(3.2.6)), the expression levels of the positive controls for MEF2C, RUNX2, ONN and PPARG2 do not show characteristic high expression levels, even though the

supporting genes in some cases show expected expression levels. This is a problem in terms of deducing the significance of the relative transcription levels.

Figure 3.17: **Transcriptional analysis of gene expression of cells cultured on PLA Honeycomb surfaces.** Data is presented as mean ± SEM. (A) shows the absolute expression levels of the housekeeping genes as well as the geometric mean. (B-H) show the lineage specific expression and (I) shows the adhesion related expression levels - all normalized to housekeeping gene and glass reference.

3.4 Pectin Scaffolds

3.4.1 Fabrication of a Pectin Scaffold

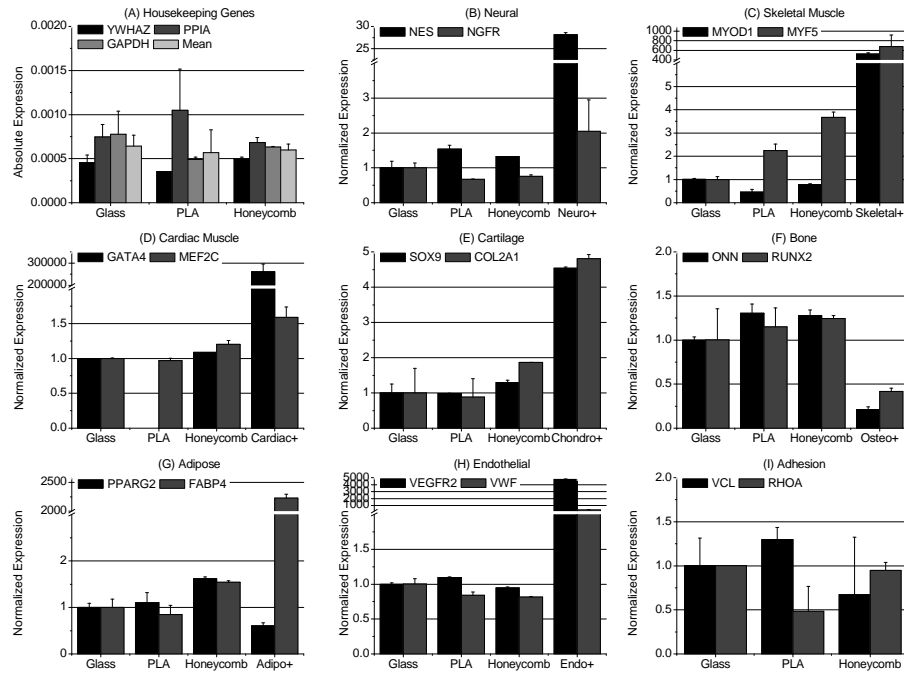Pectin alone forms a 3D network of fibers and pores, which could be very attractive to cells during cell culturing. So in order to get a first indication of the porosity of these scaffolds, pectin samples were imaged using a scanning electron microscope. The pectin samples were fabricated as described in Sec.(2.2.3) and prepared for SEM as described in Sec.(2.4).

The electron micrograph in Fig.(3.18A) reveals a spongy 3D network, where both pores and fibers were found. These pores were in the range of 30-60 μm in size, which, due to gel swelling, is anticipated to be significantly larger for the hydrated gel. The depth of the pectin scaffold can be observed in Fig.(3.18B). Fig.(3.18C) shows a high magnification image of the thin pore walls, which was estimated to be around 1 μm.

(A) 100x magnification   (B) 500x magnification   (C) 2000x magnification
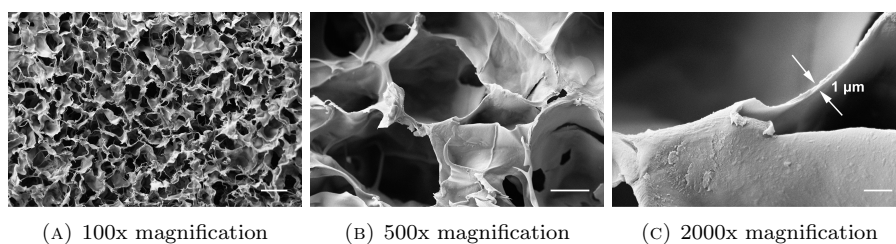
Figure 3.18: **Electron micrographs of the pure pectin scaffold.** (A) and (B) show the porosity and depth of the pectin scaffold at 100x and 500x magnification, respectively. (C) shows the pore wall thickness. Scale bars represent 100, 30 and 5 μm, respectively.

Despite the promising structure of the pectin scaffolds, they were not suitable for cell culturing in the present form due to their physicochemical properties. The scaffolds were very acidic right after fabrication (pectin solution had a pH of 3.56), and neutralization lead to disassembly of the gels. The different approaches to harness the pectin as a cell culturing scaffold can be seen in Fig.(3.19).

The first attempt to harness the pectin scaffold was to alter the concentration of pectin and Ca^{2+} as well as try to fully dehydrate the gels before use. Neither of these factors gave the desired outcome, and thus other methods had to be tried. For this reason, crosslinking with EDC/NHS, succinyl chloride, Ca^{2+} solution and combinations of these were tested. Again, neither of these achieved to stabilize the pectin scaffold at neutral pH.

The final step was to see if the pectin scaffolds could be stabilized using other polymers and thus ending up with a suitable composite gel. Agar, caprolactone and chitosan were tested as co-polymers together with pectin, and of these the agar and chitosan were promising candidates. Caprolactone had to be dissolved in chloroform, in which pectin was insoluble and thus the outcome of this mixture was grains of pectin on top of a foamy caprolactone polymer.
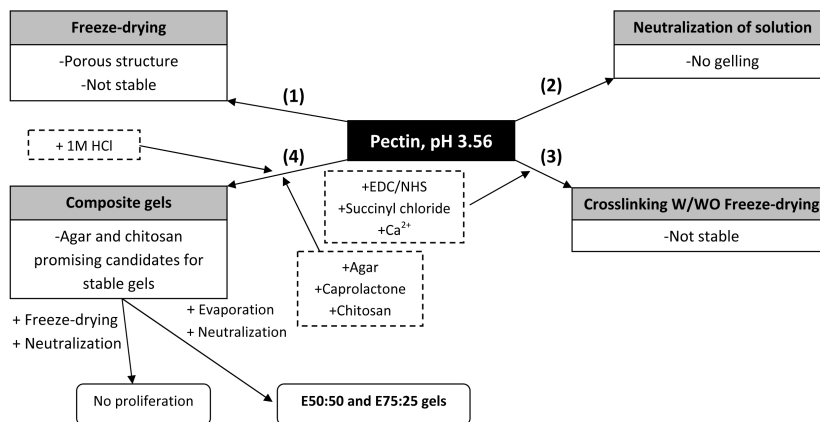
Figure 3.19: **Flowchart of the fabrication methods utilized for creating pectin scaffolds suitable for cell culturing.** Several approaches were tried to stabilize the gels for cell culturing, including freeze-drying (1), neutralization (2), crosslinking (3) and composite gelling (4).

3.4.2 Structural Analysis of Pectin-chitosan Composite Gels

Polyelectrolyte gels made of a mixture of pectin and chitosan were casted as described in Sec.(2.2.3) and further prepared for SEM. The SEM images can be seen in Fig.(3.20) and reveal macromolecular structures, which is typical for composite gels. As the amount of pectin was increased from 50% to 75% (E75:25), these macrostructures were found even more abundantly. On the contrary, the E50:50 gels demonstrate a microsized fibrous mesh. Whether these images reveal the true structure of the gels is questionable, as the preparation for SEM requires complete removal of water, which could have tremendous impact on gel structure.

3.4.3 Elasticity Analysis of the Various Surfaces

The elasticities of the different materials were evaluated using AFM in fluid contact mode. The results in Fig.(3.21) show that no difference between the glass, PST and PLA samples was observed, as these share almost similar force-extension curves. However, the pectin-chitosan composite gels clearly demonstrated their elastic properties, as the electrostatic repulsion part was dampened. Using a Hertz cone model, as described in App.(B), the Young's modulus was estimated from the measurements, which resulted in 1.3 kPa for the softer E50:50 gel and 10.8 kPa for the harder E75:25 gel, respectively.

3.4.4 Adsorption of Fibronectin to Pectin-chitosan Composite Gels

The protein adsorption to the composite gels was tested in order to get a first indication of the cell adhesion properties. The gels were coated with fibronectin, stained and imaged as described in Sec.(2.10). The results in Fig.(3.22) show that fibronectin was present on all coated surfaces. However, when comparing
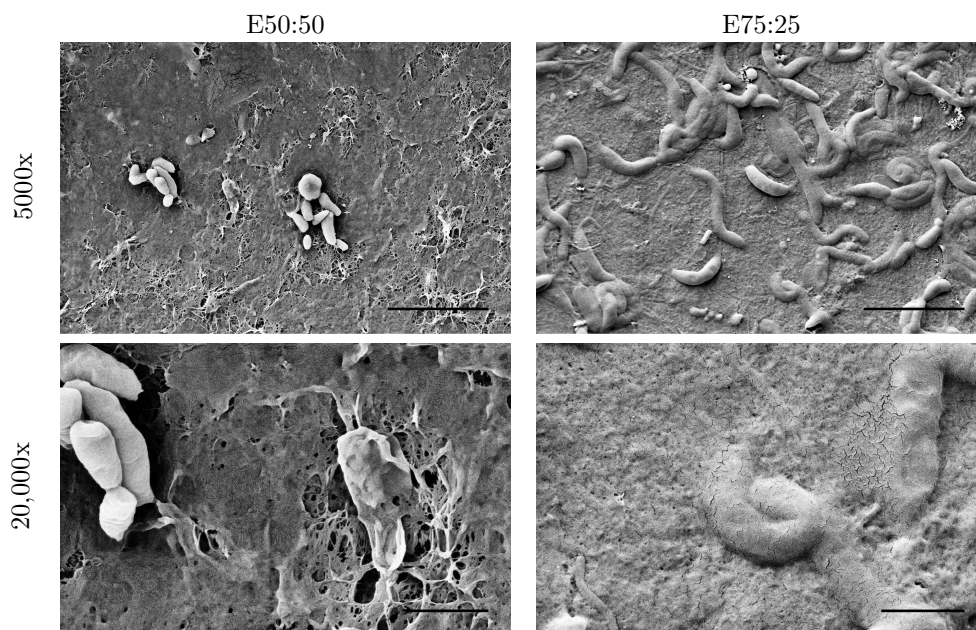
Figure 3.20: **Electron micrographs of E50:50 and E75:25 polyelectrolyte gels.** Images were obtained at 5000x and at 20,000x magnification with scale bars representing 5 μm and 1 μm, respectively.
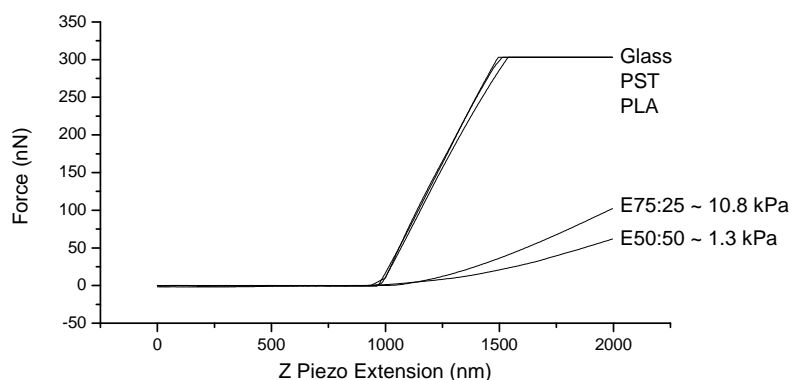
Figure 3.21: **Substrate elasticities.** Shows the force applied to the cantilever tip when approaching the different surfaces. Furthermore, the Young's modulus (calculated using the Hertz cone model) is listed for the polyelectrolyte gels.

gels to the TCPS reference, there is a clear difference in uniformness of the protein layer. The effect of pectin-to-chitosan mixing ratio does not appear to have any direct impact on the amount or distribution of the adhered fibronectin. The clustering of proteins at this scale suggests that gels have very localized features where protein can adhere. This might pose a problem for cells, as these might not be able to adhere to the surface. If they do adhere, it might be difficult for the cells to spread and cover a larger area, as gels have large protein

inert areas.
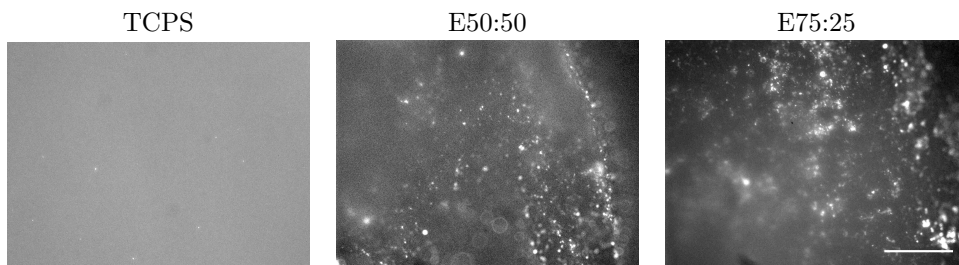
Figure 3.22: **Immunofluorescence of protein adsorption to pectin-chitosan polyelectrolyte gels.** The images show distribution of protein on TCPS, E50:50 and E75:25 surfaces. Images were obtained at 20x magnification, and scale bar represents 100 μm.

3.4.5 Spreading of Cells on Pectin-chitosan Composite Gels

The spreading of cells cultured on pectin-chitosan polyelectrolyte gels was addressed, as it is a vital step in the further development of the cells. To evaluate the spreading, gels were cut to fit a 12-well culture plate and then sterilized in 70% ethanol. ASCP9 cells were seeded at 1500 per cm^2 and cultured for 4 days, before they were fixed and stained for actin and nuclei according to the method described in Sec.(2.9). The results shown in Fig.(3.23) show that neither cells on the E50:50 or E75:25 gels spread compared to the cells on the TCPS reference. The lack of spreading of these cells could indicate that cells were not viable on these surfaces, rather they appeared apoptotic.

(A) TCPS   (B) E50:50   (C) E75:25
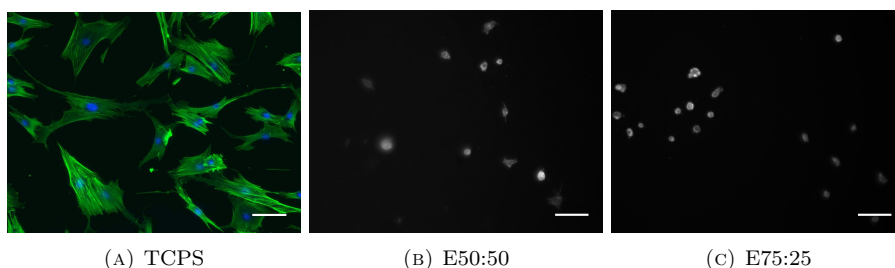
Figure 3.23: **Spreading of cells cultured on pectin-chitosan polyelectrolyte gels.** (A), (B) and (C) show actin (green) distribution (and nucleus (blue) for polystyrene) of cells cultured on polystyrene, E50:50 and E75:25 polyelectrolyte gels. Images were obtained at 10x magnification and the scale bar represents 100 μm.

3.4.6 Proliferation of Cells on Pectin-chitosan Composite Gels

To evaluate the proliferative properties of the polyelectrolyte surfaces, the metabolic activity of cells was measured. First ASCP4 cells were seeded at 1500 per cm^2 and the cell number was estimated every second day using the alamarBlue setup, as described in Sec.(2.8). The results indicate that cells on the gels did not proliferate significantly, whereas the growth curve for cells on the TCPS reference had a typical exponential shape. Furthermore, the signal from cells on the gels were below or around the limit of detection during the entire culture period, which lead to the conduction of a viability experiment instead Fig.(3.24). To test the viability, ASCP9 cells were seeded at a higher density of 5000 per cm^2, and cultured for 10 days with alamarBlue measurements every second day. This lead to a signal above the limit of detection, but as seen in the results, the cells did not proliferate on the gels. Instead it appeared as cells slowly died, as the metabolic activity of the culture steadily decreased from day 2 to day 10 - see figure inset.
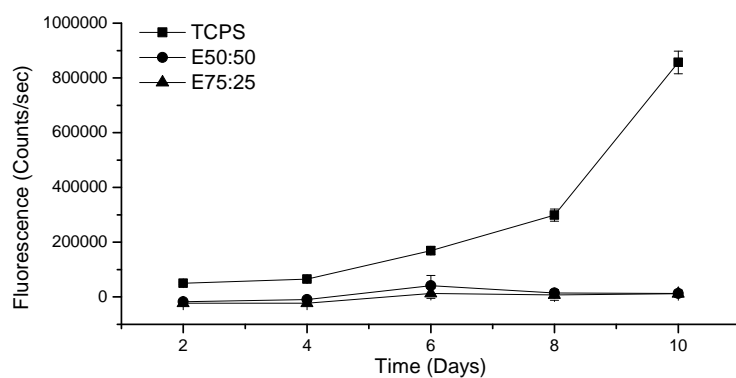
(A) Proliferation - seeding density 1500 cm^{-2}
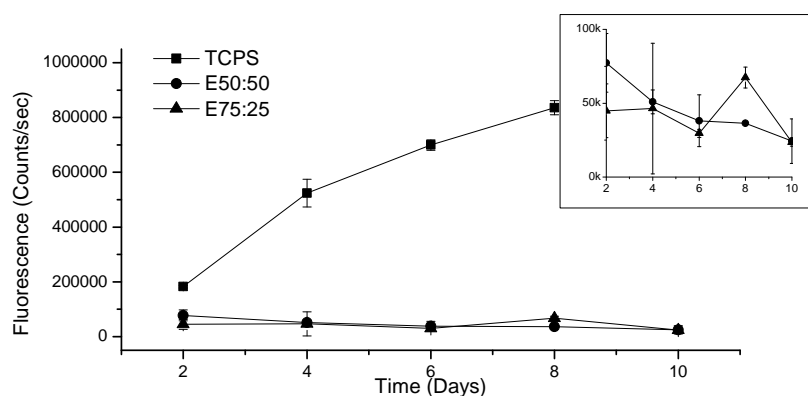
(B) Viability - seeding density 5000 cm^{-2}

Figure 3.24: **Proliferation and viability of cells on polyelectrolyte gels.**
(A) shows the proliferation, whereas (B) shows the viability of cells on polyelectrolyte gels. The inset in (B) shows a plot of the E50:50 and E75:25 metabolic activities alone. Data is represented as mean ± SEM.

4

Discussion

4.1 Discussion

4.1.1 Oxygen Plasma Etched Polystyrene

Characterization

The method for producing the oxygen plasma etched surfaces was well established by our group in a previous project. However, this method did not include varying surface roughness through control of the etching process time. In order to elucidate the effect of an increased process time, AFM and EDS measurements were conducted to probe the roughness and elemental composition at the surface, respectively. Regarding the AFM measurements, a clear correlation between surface roughness and process time was observed, which indicate that etching process time is a good parameter for controlling the substrate roughness. As seen from the images in Fig.(3.2D-F), the topography variations steadily decreased in width from micro- to nanosizes. As anticipated, the calculated effective surface area increased with increasing process time, which for the roughest surface gave an effective area that was $92 \pm 29\%$ larger than the equivalent flat surface. These alterations in topography make the plasma etched surfaces very intersting in terms of affecting the cells through the subcellular nanoregime, which has been shown by many research groups to have great impact on the cellular response [60, 61].

The elemental analysis of the etched surfaces showed that the amount of oxygen increased with increasing process time, except for the PePS10 sample as seen in Fig.(3.3). However, the deviation of this sample can be explained by a significant different topography, as the subsequent SEM analysis revealed that the surface had repolymerized. This was furthermore confirmed when the sample was examined visually, as it had a reduced transparency compared to the other samples. It should be noted that EDS is not the best suitable technique for analyzing samples that only have been modified at the surface level. This is due to the use of high energy electrons, which scatters deep (a few μm) into the substrate and thus probes a large volume. Ramsey et al [47] found that oxygen plasma treatment incorporated oxygen atoms into the substrate down to a depth of approximately 30 Å.

Protein adsorption

The altered topography and the increased surface area of the etched plates were believed to have a positive effect on the amount of protein that could be adsorbed to the surface. However, as the ELISA results in Fig.(3.4) indicate, there was a contradictory picture of this hypothesis. Coating the surface with pure fibronectin revealed that etched surfaces adsorbed equal amount of protein, independent of surface roughness. Furthermore, they showed less adsorption compared to the TCPS reference. However, when using a 10% FBS protein coating, which is a complex mixture af several proteins, the trend was reversed with etched surfaces displaying higher adsorption than the TCPS reference. In addition, the etched surfaces showed a gradual increase in adsorption as function of roughness. This contradiction could be explained by different adsorption dynamics between the two protein solutions, which might be explained by the presence of other proteins in the FBS solution that could assist in the anchorage of the fibronectin molecules. Together these results indicate that protein adsorption is influenced by some factors that were not controlled in these experiments, e.g. surface charge. Furthermore, it indicates that adsorption of proteins might be a very selective process, that is dependent on the specific protein. This hypothesis is furthermore confirmed in results published by Lord and colleagues [90], who found that fibronogen adhesion decreased with increased substrate roughness, whereas substrate roughness had no effect on fibronectin and albumin adsorption.

Spreading

The first observation regarding altered cellular responses was the morphology of the cells. The PCM images in Fig.(3.5) show no observable difference between the cells on the nanorough surfaces - neither after 24 or 96 hours. To better quantify any differences between the surfaces, cytomorphometry measurements were conducted. The results in Fig.(3.6) show that cells had a significantly different morphology based on circularity, major axis, minor axis, elongation and perimeter measurements. This could indicate that cells do respond to the roughness of the substratum. However, as there was no differences between the etched surfaces (except for the circularity), it is hard to deduce whether the cells respond to the roughness, surface charge or chemical composition of the surface. In general these results cohere with the observed protein adsorption properties, as all etched surfaces showed equally different cell morphology compared to TCPS.

When looking at the stress fiber and FA distribution of the individual cells in Fig.(3.7), it appears as the FA size decreased with increasing roughness. A possible explanation for this, could be that integrin clustering in the cells were limited due to the rapidly varying substrate. This has furthermore been observed by Kunzler et al [60], who saw less developed FAs and stress fibers in cells cultured on nanorough surfaces. Integrins are approximately 30 nm in length, and have an extracellular part which is roughly 20 nm long [91]. The plasma etched surfaces have height variations from 100-150 nm within a few hundred nm (the average peak-valley distance), meaning that intracellular clustering of integrins would require cells to curve along the substrate topography, which would require more work to deform the cell membrane.

Proliferation

Proliferation of cells cultured on the nanorough surfaces was much alike, which also was confirmed by the calculated doubling times. This is quite surprising that the altered substratum roughness did not influence the proliferation of the cells, because the altered cell spreading could very well translate into changes in proliferation through the FA-mediated signaling pathways. Hatano and colleagues [92] tested the effect of substrate roughness ($0 < R_a < 2.9 \ \mu m$) of Thermanox polystyrene slides from Nunc on proliferation and gene expression of rat calvarial cells. Their results showed that the proliferation and osteocalcin mRNA levels were only slightly higher on surfaces with $R_a = 0.81 \ \mu m$. Thus, taking the large range of roughness and the small differences in mind, it is understandable why no differences were observed for the PePS surfaces of this project, as these R_a values varied between 4-55 nm.

Dolatshahi-Pirouz and colleagues [93] tested the effect of increasing platinum nanoroughness on proliferation of human fibroblasts. Their results showed that for increasing roughness ($0 < R_{RMS} < 27 \ nm$), the proliferation gradually decreased. Interestingly, they also observed a gradual increase in fibrinogen adsorption as the surface roughness increased. This could suggest that there is a connection between cell proliferation and protein adsorption properties.

Differentiation

Spontaneous differentiation of the cells was evaluated at transcription level by real-time qPCR. The results indicate that cells responded to the nanorough surfaces by upregulating, in relation to TCPS reference, collagen II expression by a factor 2 for the PePS5 surface and a factor 3 for the PePS7 and 10 surfaces. Furthermore, RUNX2, the transcription factor involved in committing the undifferentiated MSC to the preosteoblast phenotype [32], was upregulated 1.6, 1.7 and 2.25 times for the PePS5,7 and 10, respectively, compared to the TCPS reference. In addition, the intracellular signaling molecule RhoA was upregulated by a factor 25 for cells on PePS7 and 10 surfaces. McBeath and co-workers [63] made a study to investigate the effect of cell shape on lineage commitment, and they found that well-spread cells tend to undergo osteogenesis, whereas rounded cells become adipocytes. Furthermore, their results showed that cells undergoing osteogenesis had an increased level of RhoA expression. In the scope of these findings, it could be hypothesized that increasing substrate roughness induces cells to the osteogenic lineage, and that these surfaces might demonstrate better conditions for doing in vitro osteogenesis. A recent study by Rich and colleagues [94] demonstrated that the gene COL2A1 was upregulated at day 28 under chondrogenic conditions, whereas no change was observed under osteogenesis. Whether the cells on the PePS surfaces should be undergoing chondrogenesis is highly doubtful, as no alterations in expression of the paramount chondrogenic transcription factor [95], SOX9, was observed.

The chart also showed some other alterations in gene expression, however many of these were so low compared to the positive control, that the intersample regulation is without any biological significance. It should be noted that MEF2C and PPARG2 showed decent level for the samples compared to the positive control. However, as the second gene in their group (GATA4 and FABP4, respectively) showed little or no expression in the samples compared to the control, it is difficult to deduce the meaning of these small variations. This

again addresses the general reliability of this method for "hunting" unknown expression alterations, which will be discussed in Sec.(4.1.4).

4.1.2 Honeycomb Polylactic Acid

Characterization

The first step in the utilization of these surfaces for cell culturing was to produce and characterize the surfaces. The method for producing these surfaces is straightforward and has been described by several research groups [71–73]. However, we observed that humidity had a significant impact on the honeycomb formation (from microsized to nanosized pores), and that the PLA-to-DOPE ratio only had little influence hereon (data not shown). In order to evaluate the individual pore sizes as well as the uniformity of the surface coverage, AFM and SEM images were obtained. These images, which are shown in Fig.(3.10), reveal that surfaces were covered with nanosized pores with an average diameter of $322 \pm 0.004 \ nm$. Furthermore, the profile of the pores reveals that the pore depth was $> 50 \ nm$. The formation of nanosized pores using this solvent casting method has not been reported before, whereas pore sizes ranging between 1 and $10 \ \mu m$ is the most frequent [71–73, 75, 96].

Protein adsorption

In order to elucidate if these substrate structures had any influence on the protein adsorption, indirect ELISA and immunofluorescence microscopy experiments were conducted. The ELISA results shown in Fig.(3.11) demonstrated a significant difference between the flat PLA surface and the PLA honeycomb surface for the pure fibronectin coating. Furthermore, the adsorption on the PLA honeycomb was significantly higher than that on the glass reference. Together these observations indicate that the increased protein adsorption on the PLA honeycomb surfaces, is not due to adsorption to the underlying glass substrate, but rather a response to the structure of the substratum.

The immunofluorescence results in Fig.(3.12) confirmed this hypothesis by demonstrating that the fibronectin adhered locally on the surface, and thus reflecting the honeycomb pattern of the substrate. Based on these images, which were on the verge of usable resolution, the pore size was estimated to be $432 \pm 0.010 \ nm$. These results show that a substratum topography pattern can be translated very specifically into a protein adsorption pattern, which is the key link between the substratum and cells. That fibronectin binds very site selectively has been confirmed by results obtained by Sunami et al [79], who found that fibronectin from a FBS solution adhered selectively to the microsized pores of the honeycomb films, and that BSA adhered non-specifically to both the honeycomb patterned and flat surfaces.

Spreading

The morphology of cells cultured on PLA and PLA honeycomb differs from that of cells cultured on TCPS and glass, as seen in Fig.(3.13). The difference was observable already after 24 hours of culturing, and it became more prominent after 48 and 96 hours. The cell populations on TCPS and glass were characterized by more cells spreading multi-directionally compared to those on the PLA and PLA honeycomb, which appeared more uniaxial.

The cytomorphometry analysis results in Fig.(3.14) indicate that cells cultured on PLA and PLA honeycomb covered a significantly smaller area than those cultured on glass. The circularity of cells cultured on PLA was significantly higher than that for cells cultured on glass and PLA honeycomb, which could be explained by cells having a uniaxial morphology on PLA compared to a multiaxial morphology on glass, and that cells on PLA had a wider cell body compared to those on PLA honeycomb. This hypothesis is furthermore supported by the major and minor axis results, which demonstrated that cells roughly have the same length, but significantly differed in width of the cell body. Lastly the results demonstrate that cells cultured on PLA honeycomb had a significantly higher elongation index compared to cells on the glass reference, whereas no significant difference was observed between flat PLA and glass. Together these results suggest that cells respond to the chemical change from glass to PLA, and additionally that cells respond to the topography of the PLA honeycomb surfaces.

The distribution of stress fibers and FAs in the cells was very much affected by the overall shape of the cell. This can be seen from the results in Fig.(3.15), which show a typical multi-directionally spreading cell on glass, and uniaxially spreading cells on PLA and PLA honeycomb. The uniaxial cells on PLA and PLA honeycomb were furthermore characterized by having less amount of stress fibers and less prominent FAs. In addition the cells had clearly defined leading and trailing edges, which indicate that cells had a higher level of migrating on these surfaces.

Arai and co-workers [75] demonstrated that cardiac myocytes, on various microsized honeycomb substrates (4-12 μm in diameter), differed in morphology, and that vinculin co-localized with the edge of the honeycomb pore. Furthermore, they found that cardiac myocytes cultured on the surfaces with the largest pores, went from a heterogeneous population, of multi-directionally and uniaxially spreading cells, to a more homogeneous population only consisting of uniaxial cells. That microsized pores have significant impact on cell morphology was also demonstrated by Fukuhira and colleagues [74], who reported a significantly different morphology of human chondrocytes, seeded on 5 μm wide honeycomb structures, compared to the flat reference. Together these results suggest that substratum structures in the cellular range ($\approx \mu m$) have significant impact on cell morphology, whereas alterations in the subcellular range ($\approx nm$) show less prominent morphology differences.

Proliferation

The proliferation of cells cultured on the various surfaces showed a significantly lower cell number at day 6, 8 and 10 on PLA and PLA honeycomb surfaces compared to both TCPS and glass. A possible explanation for the reduced proliferation on these surfaces could be related to decreased spreading and FA assembly of the cells, which is critical for cells to proceed in the cell cycle. Furthermore, if cells have a higher level of migration, they might shift their activity away from proliferation related cell functions in order to compensate for the increased migration activity. Fukuhira et al [74] observed that chondrocytes proliferated significantly slower on microsized PLA honeycomb films compared to the flat PLA. However, the slower proliferating chondrocytes remained a spherical shape and produced ECM more abundantly, which could

indicate that the honeycomb surfaces were better at maintaining the differentiated phenotype. This trend has also been reported for osteoblasts cultured on microsized honeycomb films by Chaudhuri and colleagues [77]. These findings, that there are observable differences between flat and honeycomb PLA, are somewhat contradictory to what is observed in this study, which again could indicate that there is a major difference in cellular responses when addressing the cellular or subcellular level.

Differentiation

The gene expression results, found in Fig.(3.17), demonstrate that no significant difference between the surfaces exist. This is interesting as the cell morphology results clearly demonstrated that cells obtained an altered morphology when cultured on PLA and PLA honeycomb. Fukuhira et al [74] showed that microsized honeycomb structures provided an environment, in which chondrocytes could maintain the differentiated phenotype. Likewise, it appears as the nanosized honeycomb pattern does not induce any differentiation of ASCs, even though they radically change their morphology. Neither does the vinculin or RhoA expression show any significant differences, which indicate that these adhesion and signaling molecules are not affected at transcription level by the altered cell morphology.

These experiments were conducted in parallel with the expression experiments for the PePS surfaces, which is reflected in the results, as these give rise to the same interpretation questions regarding MEF2C, PPARG2, ONN and RUNX2, NGFR. As already mentioned, the qPCR method will be discussed in Sec.(4.1.4).

4.1.3 Pectin Scaffolds

The pectin scaffolds proved hard to prepare so they could resist degradation under cell culture conditions. At first, SEM images of the freeze-dried pectin scaffold (Fig.(3.18)) showed a very interesting 3D structure with features spanning the supracellular, cellular and subcellular regimes. E.g pores were around 30-60 μm in diameter and pore wall thicknesses around 1 μm. This structure has also been reported by Liu et al [85]. However, as these gels were acidic with a pH around 3.5, they were not suitable for cell culturing, and neutralization made the gels disassemble. Neither of the utilized crosslinking methods were able to stabilize the structure enough to withstand several days in a cell culture environment. For this reason, co-polymer stabilization was tried using agar, caprolactone and chitosan, where the latter showed to be the best suitable candidate. It should be noted that freeze-drying of the initial polymer mixture was tried as well, and this lead to a promising scaffold that was stable during culturing. However, preliminary proliferation experiments (data not shown) demonstrated that cells did not proliferate at all in these scaffolds. The simple evaporation followed by neutralization in a water bath resulted in stable rigid gels (E50:50 and E75:25) that easily could be sliced and cut to fit a culture well.

The SEM images of these gels in Fig.(3.20) revealed a considerable different structure, that displayed both macromolecular assemblies as well as a nanosized fibrous network. The macromolecular features are typical for composite gels, and results by Bernabé and colleagues [97] show somewhat similar structures for a pectin-chitosan composite gel. Regarding the fibrous network it should be

noted, that the preparation of the gels for SEM required complete dehydration of the gels, which could lead to collapse of the structure. Therefore it is difficult to determine if the fibrous network is more frequent in the hydrated gels. In general, it is difficult to conclude anything on the structure of the gels in culture, as these are very hydrated and therefore swollen.

An interesting feature about these gels is their elasticity, which seems to be controllable through the mixing ratio of pectin and chitosan. If gels were engineered to be more cellophilic, the mixing ratio could be utilized to control the substrate elasticity, which has been shown by Engler et al [62] to influence the lineage commitment of bone marrow derived hMSCs. Their results showed that soft substrates with elasticities approximating that of neural tissue were neurogenic, whereas stiff substrates with elasticities resembling bone ECM were osteogenic.

Protein adsorption to the gels appeared to be severely reduced compared to TCPS. Furthermore, the distribution only occurred in clusters on the gel surface, which might explain the absence of spreading and proliferation on these gels. As seen from Fig.(3.23), the spreading of the cells on these surfaces was severely retarded, which could hinder the cells from progressing through the cell cycle and thereby proliferate. The viability results in Fig.(3.24) actually show that the sample fluorescence was decreasing as function of time, meaning that some cells either died or reduced their metabolic activity. That cells do not adhere very well to hydrogels has been reported by other authors as well. E.g. in a study by Rowley et al [98], alginate hydrogels were tested as scaffolds for cell culturing. Their results showed that cells could not adhere to or proliferate on the untreated alginate gels, whereas EDC/NHS crosslinking of short GRGDY peptides to the surfaces lead to complete spreading and proliferation of myoblasts.

In another study by Liu and co-workers [86], pectin-PLGA composite gels were fabricated for culturing of osteoblasts. The results showed that the number of osteoblasts were significantly higher after 14 days on pectin-PLGA gels compared to the PLGA reference. However, it should be noted that initial viability was low, as more than 60 and 70% of the cells died on the pectin-PLGA and PLGA surfaces, respectively. Furthermore, the doubling time for their cells on these scaffolds were around 14 days, which is exceptionally high compared to what other autors have reported for MC3T3-E1 osteoblasts on PLGA ($\approx$ 48 hours) [99].

4.1.4   Method and Experiment Improvements

In this study proliferation was tested using an alamarBlue setup, which has been utilized by several other research groups for estimating cell quantity under various conditions [58, 74, 100]. The sensitivity and linearity of alamarBlue were tested in this study, and the results shown in Fig.(3.1) and Tab.(3.1) show that after 4 hours of incubation, a linear correlation between number of cells and sample fluorescence was observed. However, the results also indicate that the mitochondrial activity was not constant at all times, which troubles the conversion of alamarBlue reduction to absolute number of cells. Takeda and co-workers [101] investigated the effect of culturing conditions on mitochondrial activity, and their results demonstrated that the activity was highest during the proliferative phase and significantly lowered when cells reached confluence.

The morphology of the spreading cells were quantified by cytomorphometry

measurements based on area, circularity, ellipse fitting and perimeter. Even though, these measurements provide some good indices for the cell morphology, they cannot fully describe the complex shape of a living cell. E.g. an ellipse might not be the best geometrical shape to fit to a cell with several protrusions from the cell body. In order to improve the cytomorphometry analysis, one should look into more complex parameters that can describe some of the complex features of a cell shape.

Regarding the spreading, it could also have been of interest to obtain SEM images of the cells on both the oxygen plasma etched and PLA honeycomb surfaces, as this might show how cells interact with the different structures. As an example, Dalby et al [48] used SEM to show that cells interacted specifically with 75 nm wide pits through their filopodia.

The differences in the gene expression for the cells cultured on the oxygen plasma etched surfaces should be repeated, and furthermore investigated using a wider assay of osteogenesis related genes. In addition, stainings or western blots should be done to see if the changes at transcription level translate into proteins, which would be the final proof for an altered cell phenotype. If this is the case, then these results indicate that substratum nanoroughness might be beneficial for differentiation of stem cells into osteoblasts.

In general, the utilized real-time qPCR setup for probing the alterations in gene expression might not be optimal for this purpose. This is not due to the method, rather the design of the gene assay, which included two specific genes within each lineage. However, as the results have demonstrated, there have been many problems regarding intersample expression alterations, where one gene showed decent expressions and the other showed nothing compared to the positive control. Observations like these are difficult to interpret, and thus a wider gene panel should be addressed to increase the reliability of the assay. However, this is both time consuming and very expensive, and therefore alternative methods should be investigated. RNA microarray kits can be purchased in many sizes (from a few hundred genes to several thousand), and these are fairly cheap compared to the qPCR gene assay setup. The great advantage of such a kit, is the wide spectrum of genes that is probed within each category, and thus cluster analysis of transcription differences can be performed. This would significantly improve the interpretation of any alterations in gene expression.

The PLA honeycomb surfaces provide a good model to investigate the effect of micro- versus nanotopography. By controlling casting volume, concentration, PLA-to-DOPE ratio, temperature and humidity, it should be possible to gradually increase the pore size from the nano- to the microscale. Preliminary experiments of this study show that honeycomb surfaces with pore diameters around 1-4 μm could be obtained. However, as the room humidity changed during the danish seasons, it became impossible to reproduce these surfaces. So in order to establish a fabrication method for reproducible pore sizes, a special incubation chamber, that allows the control of the aforementioned parameters, has to be built. Such a study would allow the researcher to investigate the difference in cellular responses when cells were exposed to the same type of feature in different sizes, namely from nano to microsized honeycombs.

The pectin composite gels should be engineered in another way to produce more suitable hydrogels or polyelectrolyte gels for cell culturing. Alternatively, the pectin-chitosan gels should be modified to include cell adhesion facilitating proteins on the surface. This could be short GRGDY peptides [98] or collagen

molecules [102], which both can be crosslinked to the gels through carbodiimide reactions.

5

Conclusion

The three different surfaces each showed to have an effect on ASCs in culture.

The oxygen plasma etched plates with varying roughness showed to affect the morphology of spreading cells as well as the expression of adhesion- and bone differentiation-related genes. Together these results make these surfaces interesting in terms of controlled differentiation of stem cells into bone cells, both in vitro and in vivo. These surfaces definitely have to be investigated further to confirm the changes observed in gene expression. In addition, a wider bone-related gene assay has to be probed and analysis at protein level has to be included too.

The PLA honeycomb surfaces showed to have significant impact on fibronectin adsorption and distribution. Furthermore, the cultured cells had a significantly different cell morphology compared to those on glass and flat PLA. However, despite the alteration in cell morphology, no significant changes in proliferation or gene expression were observed, which suggests that the PLA honeycomb surfaces do not facilitate spontaneous differentiation of cells in culture. In general, the most prominent differences in cell responses were observed between the glass reference and the PLA surfaces (flat or honeycomb), which indicates that the physicochemical properties of the PLA polymer have a greater impact on cells than topography has. For this reason, it could be interesting to test micro- versus nanoscaled pores, which could be used to test if some parts of the biological scale give rise to stronger topography-related responses. With the utilized method of fabrication, the pore size can easily be controlled trough casting environment conditions.

The pectin scaffolds required a lot of engineering in order to be stable for cell culturing. Despite this, these were still not very cellophilic, as cells did not spread or proliferate. In addition, the viability experiment showed that cells did in fact die on these scaffolds. Despite this, the pectin scaffolds still pose an interesting culture system, as both the structural and mechanical properties showed promising results in relation to cell culturing. It is evident that these scaffolds require further engineering for optimizing their biocompatibility as well as understanding how to control these structural and mechanical properties.

In conclusion, the results of this report demonstrate that cells do react to nanofeatures of the substratum, and that these can be utilized to control the fate

and function of ASCs. However, the responses do not appear as strong as those reported by other authors for microsized substratum features. This emphasizes the need for systematic studies where all influencing factors are identified and ultimately controlled. Under such controlled conditions it should be possible to examine the effect of one specific variable of interest, e.g. substratum feature size, feature type, overall symmetry etc.

6
Perspectives

Tissue engineering poses promising aspects for treatments involving replacement of missing or damaged tissues. This is a giant leap in modern medicine, which in combination with stem cells, make cures of otherwise debilitating diseases possible. The billion dollar investment in this research field is starting to pay off, as the world is beginning to experience incredible success stories after stem cell treatments [103]. With this being said, there is still a long way to go before researchers understand how to harness the full potential of these cells.

By investigating how cells respond to culturing conditions, being chemical or topographical, researchers can learn how to control the complex biological machinery of the human cell. That the cellular response towards a scaffold is precisely controlled is of paramount importance for taking such scaffolds into the clinic, where patient safety is top priority. By extensively studying these cell-polymer interactions, researchers become able to predict the cellular response based on the structural and physicochemical properties of a biomaterial.

The finding that cells on rougher substrata might be undergoing osteogenesis without chemical induction is promising in relation to design of osteoconductive scaffolds for bone repair. This should of course be examined further to elucidate the significance of this for osteogenesis in vitro and in vivo.

The PLA honeycomb surfaces should be investigated further before their application in tissue engineering can be stated. However, these initial experiments show that cells do not differentiate spontaneously despite they have a significantly altered cell morphology and proliferate significantly slower compared to glass and TCPS. To elaborate on these findings, more studies should be conducted, e.g. chemically induced differentiation to various cell lineages, and then measure the outcome on differentiation efficiency and final phenotype.

The pectin scaffolds should be engineered and tested further before anything can be concluded about its potential uses in tissue engineering. However, in general self-assembling hydrogel scaffolds are promising in tissue engineering due to their controllable mechanical properties as well as their ease of handling, which might be exploited for fabricating of injectable scaffolds. Furthermore, if the elasticity could be controlled trough mixing ratio with a co-polymer, injectable scaffolds, that were able to commit stem cells to a specific lineage, might be fabricated.

A

Calculation of Effective Surface Area

This script was written for MATLAB Version 7.5.0.342 (R2007b) and can be used to calculate the effective surface area of an AFM image containing x,y and z data. The principle of the calculation is to calculate and sum up the small area contributions.

```
function area = AFMSurfaceArea(filename,plot)
% AFMSurfaceArea
%**************************************************************************
%*  Calculate Effective Surface Area of an AFM Image                     *
%*  28/09-2008 by SFN                                                    *
%**************************************************************************
%Function is called by AFMSurfaceArea(filename,plot), where filename
%represents an XYZ ASCII file with 4 headerlines. The plot can either be
%left out or set to 'surf' or 'mesh', which will produce an surf or mesh
%plot, respectively. This function was designed to be compatible with AFM
%images exported from WSxM 4.0 Develop 12.21(www.nanotec.es) in the ASCII
%XYZ format.
%
%Output:
%Area, in input units.


%%
%%Load file and skip headerlines
fid = fopen(filename,'r');
C=textscan(fid, '%n %n %n', 'headerlines', 4);
fclose(fid);
%Create value matrix and design meshgrid
Img=[C{1} C{2} C{3}];
xyMin=min(Img(:,1));
xyMax=max(Img(:,1));
interval=(xyMax-xyMin)/511;
[xGrid,yGrid]=meshgrid(xyMin:interval:xyMax);
%Arrange topography information correctly
```

```matlab
for i = 1:512
    counter = i-1;
    for j = 1:512
        counter2 = counter*512 + j;
        newImg(i,j) = Img(counter2,3)/1000;
    end
end

%%
%%Calculate Surface Area
x=xGrid(1,:);                   %Vector with x-values
y=yGrid(:,1);                   %Vector with y-values
z=newImg;                       %Topography matrix in um
tempArea=0;                     %Initiate the running area variable
for i=2:length(x)
    for j=2:length(y)
        P1=[x(i-1),y(j-1),z(i-1,j-1)];  %Point 1
        P2=[x(i),y(j-1),z(i,j-1)];      %Point 2
        P3=[x(i-1),y(j),z(i-1,j)];      %Point 3
        distBase=sqrt((P2(1)-P1(1)).^2+(P2(3)-P1(3)).^2); %Length of Base
        tempVec1=cross(P2-P1,P1-P3);
        tempVec2=P2-P1;
        distHeight=sqrt(tempVec1(1).^2+tempVec1(2).^2+tempVec1(3).^2)...
            /sqrt(tempVec2(1).^2+tempVec2(2).^2+tempVec2(3).^2);    %Height
        tempArea=tempArea+distBase*distHeight;          %Area contribution
    end
end
if(nargin==2)
    if (plot=='surf')
        surf(xGrid,yGrid,newImg)
    elseif(plot=='mesh')
        mesh(xGrid,yGrid,newImg)
    end
end
area = tempArea;
```

B

Determination of Substrate Elasticity

Young's modulus (E) is the measure of the stiffness of a given material. It is one of three elastic moduli (Young's, shear and bulk), and it is defined as the tensile stress per tensile strain. The stress on a uniaxial object is given as the magnitude of the force (F) per area (A), whereas the strain is the degree of deformation, given by the ratio of the change in length (ΔL) to the original length (L_i). As long as the stress-strain relation is linear, the deformation of the object is elastic, and the object will return to its original shape if no more force is applied [104].

$$E = \frac{\text{Tensile Stress}}{\text{Tensile Strain}} = \frac{F/A}{\Delta L/L_i} \tag{B.1}$$

The general idea of using the AFM for elasticity measurements is to approach the cantilever tip to the surface of the material and monitor the force versus distance curves. From this, the total deformation can be derived as the sum of the sample deformation (indentation) and the tip deformation. To deduce the indentation from the total deformation, a reference that is infinitely stiff compared to the cantilever must be obtained. This reference material could for instance be glass [105].

The first step of the actual analysis is to align the sample curve and the reference curve properly in the same coordinate system. This must be done so the both curves have the same deflection offset (y-axis) as well as the same distance offset (x-axis) as seen in Fig.(B.1A). The indentation in the elastic specimen, as illustrated in the figure, can be calculated from:

$$\delta = d_{Reference} - d_{Sample} \tag{B.2}$$

where d is the cantilever deflection. Next the size of the force of the cantilever must be calculated using Hooke's law:

$$|F| = kd \tag{B.3}$$

where k is the spring constant of the specific cantilever. From this, a force versus indentation plot can be made as illustrated in Fig.(B.1B).

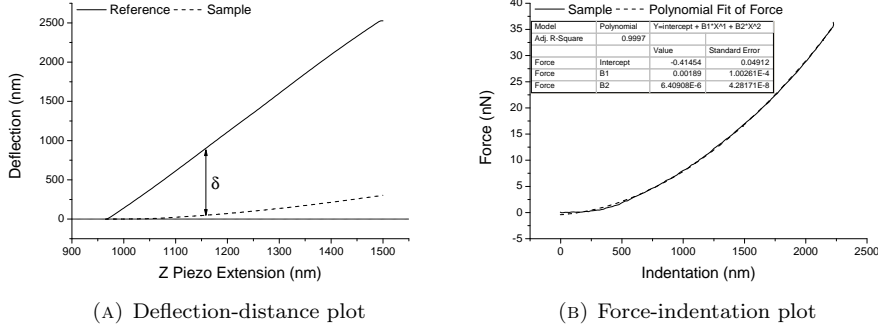(A) Deflection-distance plot (B) Force-indentation plot

Figure B.1: **Data analysis of AFM elasticity measurements.** (A) shows a typical deflection versus piezo extension plot. (B) shows the processed data in a force versus indentation plot as well as the fitted polynomial.

To extract the Young's modulus from the force-indentation plot, it is necessary to apply a Hertzian model, which describes the indentation of a non-deformable indenter (The AFM tip) into a infinitely deformable elastic material (the sample). Basically there are two models for describing the AFM tip geometry, namely the cone and paraboloid scenario.

$$F_{\text{cone}} = \frac{2}{\pi}\tan(\alpha)E^*\delta^2 \tag{B.4}$$

$$F_{\text{paraboloid}} = \frac{4}{3}E^*R^{1/2}\delta^{3/2} \tag{B.5}$$

Here F is the load force, α is the half opening angle of the conical tip, E^* is the surface elastic constant of the material, δ is the indentation depth and R is the radius of the curvature of the spherical tip. The Young's modulus (E) is given by:

$$E = E^*(1 - \nu^2) \tag{B.6}$$

Where ν is the Poisson's ratio, which for most soft materials is around 0.5 [106].

Example of calculation

The example continues with the data plotted in Fig.(B.1), which has been obtained using an Veeco NP-S10 0.12N/m cantilever that has a half opening angle $\alpha = 35°$.

From Eq.(B.4), we see that the load force is proportional indentation depth squared, meaning that the data in Fig.(B.1B) has to be fitted to a parabola. This results in a fitted coefficient $B2 = 6.40908 \times 10^{-6}$. Applying this to Eg.(B.4)

yields:

$$
\begin{aligned}
F_{\text{cone}} = \frac{2}{\pi}\tan(\alpha)E^*\delta^2 &= B2 * \delta^2 \Downarrow \\
\frac{2}{\pi}\tan(\alpha)E^* &= B2 \Downarrow \\
E^* &= B2\frac{\pi}{2\tan(\alpha)}
\end{aligned}
$$

Combining this with Eq.(B.6) yields:

$$
\begin{aligned}
E &= E^*(1-\nu^2) \\
&= B2\frac{\pi}{2\tan(\alpha)}(1-\nu^2) \\
&= 6.40908 * 10^{-6}\frac{\pi}{2\tan(35^\circ)}(1-(0.5)^2) \\
&= 1.07833 * 10^{-5}\, GPa \\
&= 10.78\, kPa
\end{aligned}
$$

Thus the Young's modulus of this sample is in the order of $\underline{10.8\ kPa}$.

C

List of Materials, Chemicals and Equipment

Materials

Description	Manufacturer	Catalog No.
Aluminum stubs for SEM	Agar Scientific	G301F
Conductive carbon tabs for SEM	Agar Scientific	G3337N
Dako Pen	DAKO	S2002
Lab-Tek II chamber slides	Nunc	154526
Metal jackets for AFM	Electron Microscopy Sciences	75010-15
SuperFrost glass slides	Menzel-Gläser	N/A
TCPS multiwell plates	Corning Costar	3598

Chemicals

Description	Manufacturer	Catalog No.
α-MEM + Glutamax	Gibco	32561-029
Agar	Fisher Scientific	Fic-A/1080/53
Anti-fibronectin AB, mouse monoclonal	Sigma	F0791
Anti-mouse AB, Alexa 488, goat	Invitrogen	A11001
Anti-mouse AB, HRP labeled, rabbit polyclonal	DAKO	P0260
Anti-rabbit AB, Cy5 labelled goat polyclonal	Chemicon	AP132S
Anti-vinculin AB, rabbit polyclonal	Sigma	V4139
alamarBlue	Biosource int.	DAL1025
Bovine serum albumin	Europe Bioproducts	BAH62-673
Calcium Chloride dihydrate	Merck	1.02382.0500
Caprolactone	Perstorp UK	CAPA 6506
cDNA synthesis kit, iScript	Bio Rad	170-8891
Chitosan	Sigma	448877
Chloroform, 99.8%	Aldrich	31998-8
DOPE, 1,2-dioleoyl-sn-glycero-3-phosphoethanolamine	Avanti Lipids	850725

Description	Manufacturer	Catalog No.
EDC, N-(3-Dimethylaminopropyl)-N-ethylcarbodiimide hydrochloride	Sigma	E7750-25G
EDTA	Bie&Berntsen	1.08418.0250
Epoxy, Hysol 3423 A&B	Loctite	33063
Fetal bovine serum	Invitrogen	10106-169
Fibronectin, Bovine	Sigma	F1141
Formaldehyde 4%	Bie&Berntsen	LAB92555
Gentamicin 10mg/ml	Invitrogen	15710-049
Hoechst 33342	Invitrogen	H3570
NHS, N-hydroxysuccinimide	Fluka	56480
OPD tablets	DAKO	S2045
Penicillin / Streptomycin	Invitrogen	15140-122
Perhydrol 30%	Merck	107209
Phalloidin, Bodipy 558/568	Molecular Probes	B3475
Phosphate buffered saline	Gibco	14200-067
PicoGreen dsDNA kit	Molecular Probes	P-7589
Polylactic Acid, Mw 60,000	Aldrich	38534
Ribonuclease Inhibitor, Human	Sigma	R2520-20KU
SDS, Sodium Dodecyl Sulfate	Sigma	L6026
Succinyl chloride	Sigma	S645-2
Sulfuric Acid 1M	Bie&Berntsen	LAB00531
TE buffer, 100x	Sigma	T9285
Total RNA mini kit	Bio-Rad	732-6820
Triton X-100	Sigma	X-100
Trypsin, 10x	Invitrogen	15090-046
Tween 20	ACROS ORGANICS	233762500

Equipment

Description	Model	Manufacturer
Atomic Force Microscope	Nanoscope IIIa	Veeco/Digital Instruments
-Cantilever for tapping	AC-160-TS	Olympus
-Cantilever for force	NP-S10	Veeco
Freeze-dryer	Alpha 1-4 LSC	Christ
Microplate reader	Victor^2 1420 multilabel counter	Wallac
Microscope, upright	BX61	Olympus
Microscope, inverted cell	Axio Observer	Zeiss
PCR thermo cycler	GeneAmp PCR system 2400	Perkin Elmer
Plasma Etcher	Rie 320 PC	Surface Technology Systems
Real-time qPCR system	MyIQ iCycler system	Bio-Rad
Scanning electron microscope	1540 XB	Zeiss
Spectrophotometer	NanoDrop 1000	Thermo Scientific
Sputter coater	S150B	Edwards

Bibliography

[1] Igor E. Konstantinov. In search of Alexander A. Maximow: The man behind the unitarian theory of hematopoiesis. *Perspectives in Biology and Medicine*, 43(2):269–276, 2000.

[2] Department of Health and Human Services. *Stem Cells: Scientific Progress and Future Research Directions*, June 2001. http://stemcells.nih.gov/info/scireport/2001report.

[3] Wagers A. J. and Weissman I. L. Plasticity of adult stem cells. *Cell*, 116(5):639–648, 2004.

[4] Department of Health and Human Services. *Stem Cell Basics*, 2006. http://stemcells.nih.gov/info/basics/basics1.

[5] Kolf C. M., Cho E., and Tuan R. S. Biology of adult mesenchymal stem cells: Regulation of niche, self-renewal and differentiation. *Arthritis Research & Therapy*, 9(1):204–214, 2007.

[6] Gimble J. M. and Guilak F. Adipose-derived adult stem cells: Isolation, characterization, and differentiation potential. *Cytotherapy*, 5(5):362–369, 2003.

[7] Zuk P. A., Zhu M., Ashjian P., Ugarte D. A. D., Huang J. I., Mizuno H., Alfonso Z. C., Fraser J. K., Benhaim P., and Hedrick M. H. Human adipose tissue is a source of multipotent stem cells. *Molecular Biology of the Cell*, 13(12):4279–4295, 2002.

[8] Pountos I. and Giannoudis P. V. Biology of mesenchymal stem cells. *Injury*, 36(3):8–12, 2005.

[9] Ratajczak M. Z., Zuba-Surma E. K., Wysoczynski M., Wan W., Ratajczak J., Wojakowski W., and Kucia M. Hunt for pluripotent stem cell - Regenerative medicine search for almighty cell. *Journal of Autoimmunity*, 30(3):151–162, 2008.

[10] Aust L., Devlin B., Foster S. J., Halvorsen Y. D. C., Hicok K., Du Laney T., Sen A., Willingmyre G. D., and Gimble J. M. Yield of human adipose-derived adult stem cells from liposuction aspirates. *Cytotherapy*, 6(1):7–14, 2004.

[11] Saltzman W. M. *Tissue Engineering: Engineering Principles for the Design of Replacement Organs and Tissues 1st Ed.* Oxford University Press, 2004.

[12] Martínez E., Engel A., Planell J.A., and Samitier J. Effects of artificial micro- and nano-structured surfaces on cell behaviour. *Annals of Anatomy*, 191(1):126–135, 2009.

[13] Abrams G. A., Goodman S. L., Nealey P. F., Franco M., and Murphy C. J. Nanoscale topography of the basement membrane underlying the corneal epithelium of the rhesus macaque. *Cell Tissue Research*, 299(1):39–46, 2000.

[14] Ringe J., Kaps C., Burmester G-R, and Sittinger M. Stem cells for regenerative medicine: Advances in the engineering of tissues and organs. *Naturwissenschaften*, 89(8):338–351, 2002.

[15] Anthony Atala. Tissue engineering and regenerative medicine: Concepts for clinical application. *Rejuvenation Research*, 7(1):15–31, 2004.

[16] Palsson B. O. and Bhatia S. N. *Tissue Engineering 1t Ed.* Prentice Hall, 2003.

[17] Lanza R., Langer R., and Vacanti J. *Principles of Tissue Engineering, 3rd ed.* Academic Press, 2007.

[18] Lodish H., Berk A., Matsudaira P., Kaiser C. A., Krieger M., Scott M. P., Zipursky S. L., and Darnell J. *Molecular Cell Biology, 5th Ed.* Freeman, 2004.

[19] Junqueira L.C and Carneiro J. *Basic Histology 11th Ed.* McGraw Hill, 2005.

[20] Wozniak M. A., Modzelewska K., Kwong L., and Keely P. J. Focal adhesion regulation of cell behavior. *Biochemica et Biophysica Acta*, 1692(2-3):103–119, 2004.

[21] Sastry S. K. and Burridge K. Focal adhesions: A nexus for intracellular signaling and cytoskeletal dynamics. *Experimental Cell Research*, 261(1):25–36, 2000.

[22] Bradshaw R. A. and Dennis E. A. *Handbook of Cell Signaling Volume 1-3.* Academic Press, 2003.

[23] Burridge K. and Chrzanowska-Wodnicka M. Focal adhesions, contractility, and signaling. *Annual Review of Cell and Developmental Biology*, 12(1):463–519, 1996.

[24] Mofrad M. R. K. and Kamm R. D. *Cytoskeletal Mechanics - Models and Measurements*. Cambridge University Press, 2006.

[25] Schwartz M. A. and Shattil S. J. Signaling networks linking integrins and Rho family GTPases. *Trends in Biochemical Sciences*, 25(8):388–391, 2000.

[26] Martin K. H., Slack J. K., Boerner S. A., Martin C. C., and Parsons J. T. Integrin connections map: To infinity and beyond. *Science*, 296(5573):1652–1653, 2002.

[27] Chen Z., Gibson T. B., Robinson F., Silvestro L., Pearson G., Xu B-e, Wright A., Vanderbilt C., and Cobb M. H. Map kinases. *Chemical Reviews*, 101(8):2449–2476, 2001.

[28] Johnson G. L. and Lapadat R. Mitogen-activated protein kinase pathways mediated by ERK, JNK, and p38 protein kinases. *Science*, 298(5600):1911–1912, 2002.

[29] Qi M. and Elion E. A. Map kinase pathways. *Journal of Cell Science*, 118(16):3569–3572, 2005.

[30] Larsen M., Artym V. V., Green J. A., and Yamada K. M. The matrix reorganized: Extracellular matrix remodeling and integrin signaling. *Current Opinion in Cell Biology*, 18(5):463471, 2006.

[31] Schwartz M. A. and Ginsberg M. H. Networks and crosstalk: Integrin signalling spreads. *Nature Cell Biology*, 4(4):E65–E68, 2002.

[32] Satija N. K., Gurudutta G. U., Sharma S., Afrin F., Gupta P., Verma Y. K., Singh V. K., and Tripathi R. P. Mesenchymal stem cells: Molecular targets for tissue engineering. *Stem Cells and Development*, 16(1):7–23, 2007.

[33] Dedhar S. Cell-substrate interactions and signaling through ILK. *Current Opinion in Cell Biology*, 12(2):250–256, 2000.

[34] Wederell E. D. and de Iongh R. U. Extracellular matrix and integrin signaling in lens development and cataract. *Seminars in Cell & Developmental Biology*, 17(6):759–776, 2006.

[35] Norman J. J. and Desai T. A. Methods for fabrication of nanoscale topography for tissue engineering scaffolds. *Annals of Biomedical Engineering*, 34(1):89–101, 2006.

[36] Lim J. Y. and Donahue H. J. Cell sensing and response to micro- and nanostructured surfaces produced by chemical and topographic patterning. *Tissue Engineering*, 13(8):1879–1891, 2007.

[37] Chen Y. and Pépin A. Nanofabrication: Conventional and nonconventional methods. *Electrophoresis*, 22(1):187–207, 2001.

[38] Lu Y. and Chen S. C. Micro and nanofabrication of biodegradable polymers for drug delivery. *Advanced Drug Delivery Reviews*, 56(11):1621 – 1633, 2004.

[39] Harrington D. A., Sharma A. K., Erickson B. A., and Cheng E. Y. Bladder tissue engineering through nanotechnology. *World Journal of Urology*, 26(4):315–322, 2008.

[40] Curtis A. and Wilkinson C. Nanotechniques and approaches in biotechnology. *Materials Today*, 4(3):232–238, 2001.

[41] Dalby M. J., Riehle M. O., Johnstone H., Affrossman S., and Curtis A. S. G. In vitro reaction of endothelial cells to polymer demixed nanotopography. *Biomaterials*, 23(14):29452954, 2002.

[42] Smith L. A. and Ma P. X. Nanofibrous scaffold for tissue engineering. *Colloids and Surfaces B: Biointerfaces*, 3(10):125–131, 2004.

[43] Campbell S. A. *The Science and Engineering of Microelectronic Fabrication, 2nd Ed.* Oxford University Press, 2001.

[44] Vieu C., Carcenac F., Ppin A., Chen Y., Mejias M., Lebib A., Manin-Ferlazzo L., Couraud L., and Launois H. Electron beam lithography: Resolution limits and applications. *Applied surface science*, 164(1-4):111–117, 2000.

[45] Mathews J. A., Wnek G. E., Simpson D. G., and Bowlin G. L. Electrospinning of collagen nanofibers. *Biomacromolecules*, 3(2):232–238, 2002.

[46] Barker S. L. and LaRocca P. J. Method of production and control of a commercial tissue culture surface. *Tissue Culture Methods*, 16(3-4):151–153, 1994.

[47] Ramsey W. S., Hertl W., Nowlan E. D., and Binkowski N. J. Surface treatments and cell attachment. *In Vitro*, 20(10):802–808, 1984.

[48] Dalby M. J., Nikolaj G., Riehle M. O., Wilkinson C. D. W., and Curtis A. S. G. Investigating filopodia sensing using arrays of defined nano-pits down to 35 nm diameter in size. *International Journal of biochemistry and Cell biology*, 36(10):2005–2015, 2004.

[49] Li W-J., Laurencin C. T., Caterson E. J., Tuan R. S., and Ko F. K. Electrospun nanofibrous structure: A novel scaffold for tissue engineering. *Journal of biomedical materials research*, 60(4):613–621, 2002.

[50] Dalby M. J., Giannaras D., Riehle M. O., Nikolaj G., Affrossman S., and Curtis A. S. G. Rapid fibroblast adhesion to 27 nm high polymer demixed nanotopography. *Biomaterials*, 25(1):77–83, 2004.

[51] Tysseling-Mattiace V. M., Sahni V., Niece K. L., Birch D., Gzeisler C., Fehlings M. G., Stupp S. I., and Kessler J. A. Self-assembling nanofibers inhibit glial scar formation and promote axon elongation after spinal cord injury. *The journal of neuroscience*, 28(14):3814–3823, 2008.

[52] Flemming R. G., Murphy C. J., Abrams G. A., Goodman S. L., and Nealey P. F. Effects of synthetic micro- and nano-structured surfaces on cell behavior. *Biomaterials*, 20(6):573–588, 1999.

[53] Wilkinson C. D. W., Riehle M., Wood M., Gallagher J., and Curtis A. S. G. The use of materials patterned on a nano- and micro-metric scale in cellular engineering. *Materials Science and Engineering C*, 19(1):263269, 2002.

[54] Wang X., Ohlin C. A., Lu Q., and Hu J. Cell directional migration and oriented division on three-dimensional laser-induced periodic surface structures on polystyrene. *Biomaterials*, 29(13):20492059, 2008.

[55] Wood A. Contact guidance on microfabricated substrata: The response of teleost fin mesenchyme cells to repeating topographical patterns. *Journal of Cell Science*, 90(4):667–681, 1988.

[56] Loesberg W. A., Riet J. te, van Delft F.C.M.J.M, Schn P., Figdor C. G., Speller S., van Loon J.J.W.A., Walboomers X. F., and Jansen J. A. The threshold at which substrate nanogroove dimensions may influence fibroblast alignment and adhesion. *Biomaterials*, 28(27):3944–3951, 2007.

[57] Berry C. C., Campbell G., Spadiccino A., Robertson M., and Curtis A. S. G. The influence of microscale topography on fibroblast attachment and motility. *Biomaterials*, 25(26):5781–5788, 2004.

[58] Choi C-H., Hagvall S. H., Wu B. M., Dunn J. C. Y., Beygui R. E., and Kim C-J. Cell interaction with three-dimensional sharp-tip nanotopography. *Biomaterials*, 28(9):1672–1679, 2007.

[59] Popat K. C., Chatvanichkul K-I., Barnes G. L., Latempa Jr. T. J., Grimes C. A., and Desai T. A. Osteogenic differentiation of marrow stromal cells cultured on nanoporous alumina surfaces. *Journal of biomedical materials research part A*, 80A(4):955–964, 2007.

[60] Kunzler T. P., Huwiler C., Drobek T., Vrs J., and Spencer N. D. Systematic study of osteoblast response to nanotopography by means of nanoparticle-density gradients. *Biomaterials*, 28(33):5000–5006, 2007.

[61] Dalby M. J., Gadegaard N., Tare R., Andar A., Riehle M. O., Herzyk P., Wilkinson C. D. W., and Oreffo R. O. C. The control of human mesenchymal cell differentiation using nanoscale symmetry and disorder. *Nature Materials*, 6(12):997–1003, 2007.

[62] Engler A. J., Sen S., Sweeney H. L., and Discher D. E. Matrix elasticity directs stem cell lineage specification. *Cell*, 126(4):677–689, 2006.

[63] McBeath R., Pirone D. M., Nelson C. M., Bhadriraju K., and Chen C. S. Cell shape, cytoskeletal tension, and RhoA regulate stem cell lineage commitment. *Developmental Cell*, 6(4):483–495, 2004.

[64] Leong N. L., Jiang J., and Lu H. H. Polymer-ceramic composite scaffold induces osteogenic differentiation of human mesenchymal stem cells. *Proceedings of the 28th IEEE conference*, pages 2651–2654, 2006.

[65] Chinn J. A., Horbett T. A., and Ratner B. D. Laboratory preparation of plasticware to support cell culture. *Journal of Tissue Culture Methods*, 16(3-4):155–159, 1994.

[66] Johansson B-L., Larsson A., Ocklind A., and Öhrlund Å. Characterization of air plasma-treated polymer surfaces by ESCA and contact angle measurements for optimization of surface stability and cell growth. *Journal of Applied Polymer Science*, 86(10):2618–2615, 2002.

[67] van Kooten T. G., Spijker H. T., and Busscher H. J. Plasma-treated polystyrene surfaces: Model surfaces for studying cell-biomaterial interactions. *Biomaterials*, 25(10):1735–1747, 2004.

[68] Petersen M., Løjkner L. D., and Nielsen S. F. Influence of bioorganic surfaces and hypoxia on proliferation of adipose tissue derived stem cells. Semester project by group 858a at the Department of Health Science and Technology, Aalborg University, 2008.

[69] Drumright R. E., Gruber P. R., and Henton D. E. Polylactic acid technology. *Advanced Materials*, 20(23):1841–1846, 2000.

[70] Ji-Dong Gu. Microbiological deterioration and degradation of synthetic polymeric materials: Recent research advances. *International deterioration and Biodegradation*, 52(2):69–91, 2003.

[71] Widawski G., Rawiso M., and Francois B. Selforganized honeycomb morphology of starpolymer polystyrene films. *Nature Letters*, 369(6479):386–389, 1994.

[72] Shimomura M. and Sawadaishi T. Bottom-up strategy of materials fabrication: A new trend in nanotechnology of soft materials. *Current Opinion in Colloid & Interface Science*, 6(1):11–16, 2001.

[73] Fukuhira Y., Kitazono E., Hayashi T., Kaneko H., Tanaka M., Shimomura M., and Sumi Y. Biodegradable honeycomb-patterned film composed of poly(lactic acid) and dioleoylphosphatidylethanolamine. *Biomaterials*, 27(9):1797–1802, 2006.

[74] Fukuhira Y., Kaneko H., Yamaga M., Tanaka M., Yamamoto S., and Shimomura M. Effect of honeycomb-patterned structure on chondrocyte behavior in vitro. *Colloids and Surfaces A: Physicochemical and Engineering Aspects*, 313-314:520–525, 2008.

[75] Arai K., Tanaka M., Yamamoto S., and Shimomura M. Effect of pore size of honeycomb films on the morphology, adhesion and cytoskeletal organization of cardiac myocytes. *Colloids and Surfaces A: Physicochemical and Engineering Aspects*, 313-314:530–535, 2008.

[76] Tanaka M., Nishikawa K., Okubo H., Kamachi H., Kawai T., Matsushita M., Todo S., and Shimomura M. Control of hepatocyte adhesion and function on self-organized honeycomb-patterned polymer film. *Colloids and Surfaces A: Physicochemical and Engineering Aspects*, 284-285:464–469, 2006.

[77] Chaudhuri J. B., Davidson M. G., Ellis M. J., Jones M. D., and Wu X. Fabrication of honeycomb-structured poly(dl-lactide) and poly [(dl-lactide)-co-glycolide] films and their use as scaffolds for osteoblast-like cell culture. *Macromolecular symposia*, 272(1):52–57, 2008.

[78] Yamamoto S., Tanaka M., Sunami H., Arai K., Takayama A., Yamashita S., Morita Y., and Shimomura M. Relationship between adsorbed fibronectin and cell adhesion on a honeycomb-patterned film. *Surface Science*, 600(18):3785–3791, 2006.

[79] Sunami H., Ito E., Tanaka M., Yamamoto S., and Shimomura M. Effect of honeycomb film on protein adsorption, cell adhesion and proliferation. *Colloids and Surfaces A: Physicochemical and Engineering Aspects*, 284-285:548–551, 2006.

[80] Drury J. L. and Mooney D. J. Hydrogels for tissue engineering: Scaffold design variables and applications. *Biomaterials*, 24(24):4337–4351, 2003.

[81] Kopecek J. Hydrogel biomaterials: A smart future? *Biomaterials*, 28(34):5185–5192, 2007.

[82] Sungthongjeen S., Sriamornsak P., Pitaksuteepong T., and Somsiri A. Effect of degree of esterification of pectin and calcium amount on drug release from pectin-based matrix tablets. *AAPS PharmSciTech*, 5(1):Article 9, 2004.

[83] Yoshimura T., Sengoku K., and Fujioka R. Pectin-based superabsorbent hydrogels crosslinked by some chemicals: Synthesis and characterization. *Polymer Bulletin*, 55(1-2):123–129, 2005.

[84] El-Nawawi S. A. and Heikal Y. A. Factors affecting the production of low-ester pectin gels. *Carbohydrate Polymers*, 26(3):189–193, 1995.

[85] Liu L., Cooke P. H., Coffin D. R., Fishman M. L., and Hicks K. B. Pectin and polyacrylamide composite hydrogels: Effect of pectin on structural and dynamic mechanical properties. *Journal of Applied Polymer Science*, 92(3):1893–1901, 2004.

[86] Liu L., Won Y. J., Cooke P. H., Coffin D. R., Fishman M. L., Hicks H. B., and Ma P. X. Pectin/poly(lactide-co-glycolide) composite matrices for biomedical applications. *Biomaterials*, 25(16):3201–3210, 2004.

[87] Horcas I., Fernndez R., Gmez-Rodrguez J.M., Colchero J., Gòmez-Herrero J., and Baro A.M. WSxM: A software for scanning probe microscopy and a tool for nanotechnology. *Review of Scientific Instruments*, 78(1), 2007.

[88] Zuk P. A., Zhu M., Mizuno H., Huang J. I., Futrell W., Katz A. J., Benhaim P., Lorenz P., and Hedrick M. H. Multilineage cells from adipose tissue: Implications for cell-based therapies. *Tissue Engineering*, 7(2):211–228, 2001.

[89] Rengarajan K., Cristol S. M., Mehta M., and Nickerson J. M. Quantifying DNA concentrations using fluorometry: A comparison of fluorophores. *Molecular Vision*, 8:416–421, 2002.

[90] Lord M. S., Cousins B. G., Doherty P. J., Whitelock J. M., Simmons A., Williams R. L., and Milthorpe B. K. The effect of silica nanoparticulate coatings on serum protein adsorption and cellular response. *Biomaterials*, 27(28):4856–4862, 2006.

[91] Alberts A., Johnson A., Lewis J., Raff M., Roberts K., and Walter P. *Molecular Biology of the Cell 4th Ed.* Garland Sciences, 2002.

[92] Hatano K., Inoue H., Kojo T., Matsunaga T., Tsujisawa T., Uchiyama C., and Uchida Y. Effect of surface roughness on proliferation and alkaline phosphatase expression of rat calvarial cells cultured on polystyrene. *Bone*, 25(4):439–445, 1999.

[93] Dolatshahi-Pirouz A., Pennisi C. P., Skeldal S., Foss M., Chevallier J., Zachar V., Andreasen P., Yoshida K., and Besenbacher F. The influence of glancing angle deposited nano-rough platinum surfaces on the adsorption of fibrinogen and the proliferation of primary human fibroblasts. *Nanotechnology*, 20(9):095101 (9pp), 2009.

[94] Rich J. T., Rosová I., Nolta J. A., Myckatyn T. M., Sandell L. J., and McAlinden A. Upregulation of Runx2 and osterix during in vitro chondrogenesis of human adipose-derived stromal cells. *Biochemical and Biophysical Research Communications*, 372(1):230–235, 2008.

[95] Betre H., Ong S. R., Guilak F., Chilkoti A., Fermor B., and Setton L. A. Chondrocytic differentiation of human adipose-derived adult stem cells in elastin-like polypeptide. *Biomaterials*, 27(1):91–99, 2006.

[96] Tian Y., Ding H., Jiao Q., and Shi Y. Influence of solvents on the formation of honeycomb films by water droplets templating. *Macromolecular Chemistry and Physics*, 207(5):530–535, 2006.

[97] Bernabé P., Peniche C., and Arüelles-Monal W. Swelling behavior of chitosan/pectin polyelectrolyte complex membranes. Effect of thermal crosslinking. *Polymer Bulletin*, 55(5):367–375, 2005.

[98] Rowley J. A., Madlambayan G., and Mooney D. J. Alginate hydrogels as synthetic extracellular matrix materials. *Biomaterials*, 20(1):45–53, 1999.

[99] Elgendy H. M., Norman M. E., Keaton A. R., and Laurencin C. T. Osteoblast-like cell (MC3T3-E1) proliferation on bioerodible polymers: An approach towards the development of a bone-bioerodible polymer composite material. *Biomaterials*, 14(4):263–269, 1993.

[100] Tan W., Krishnaraj R., and Desai T. A. Evaluation of nanostructured composite collagen-chitosan matrices for tissue engineering. *Tissue Engineering*, 7(2):203–210, 2001.

[101] Takeda K., Akagi S., Takahashi S., Onishi A., Hanada H., and Pinkert C. A. Mitochondrial activity in response to serum starvation in bovine (bos taurus) cell culture. *Cloning and Stem Cells*, 4(3):223–229, 2002.

[102] Rafat M., Li F., Fagerholm P., Lagali N. S. Watsky M. A., Munger R., Matsuura T., and Griffith M. PEG-stabilized carbodiimide crosslinked collagen-chitosan hydrogels for corneal tissue engineering. *Biomaterials*, 29(29):3960 – 3972, 2008.

[103] China Stem Cells. China stem cell news, May 2009. http://www.stemcellschina.com.

[104] Serway R. A. and Jewett J. W. *Physics for Scientists and Engineers with Modern Physics 6th Ed.* Thompson Books/Cole, 2004.

[105] Vinckier A. and Semenza G. Measuring elasticity of biological materials by atomic force microscopy. *FEBS Letters*, 430(1-2):12–16, 1998.

[106] Tauhami A., Nysten B., and Dufrne Y. F. Nanoscale mapping of the elasticity of microbial cells for atomic force microscopy. *Langmuir*, 19(11):4539–4543, 2003.